A Constrained Bayesian Optimization Framework for Structural Vibrations with Local Nonlinearities

Quentin Ragueneau, Luc Laurent, Antoine Legay, Thomas Larroque, Romain Crambuer

A Constrained Bayesian Optimization Framework for Structural Vibrations with Local Nonlinearities

Quentin RAGUENEAU[a,b,c]
Luc LAURENT[a,b]
Antoine LEGAY[a,b]
Thomas LARROQUE[c]
Romain CRAMBUER[c]

[a] Laboratoire de Mécanique des Structures et des Systèmes Couplés, Conservatoire national des arts et métiers, case courrier 2D6R10, 2 rue Conté, 75003 Paris, France
Tel.: +33-1-58-80-85-80
luc.laurent@lecnam.net & antoine.legay@lecnam.net
[b] HESAM University, 75005, Paris, France
[c] INGELIANCE Technologies, 33700, Mérignac, France
quentin.ragueneau@ingeliance.com & romain.crambuer@ingeliance.com

Abstract

In order to address stringent standards, energy efficiency objectives or also cost reduction imperatives, the optimal design of complex industrial structures is an important concern. In this context, parametric optimization offers a powerful tool for engineers. Taking into account nonlinear behavior in the models allows performing high-fidelity numerical simulations and thus reducing safety margins. However, in vibration dynamics, the use of classical global optimization methods on industrial-scale structures with nonlinearities is not affordable due to too many required solver calls to localize the optimum. This work proposes an approach to achieve global constrained optimization of structures with local nonlinearities in vibration. The strategy is based on a Bayesian Optimization process relying on two tools: (i) a Gaussian Process as a surrogate model and (ii) a dedicated nonlinear mechanical solver based on the Harmonic Balance Method. These two tools are presented in detail. Their performance and characteristics are presented and analyzed on academic and industrial-scale examples. The whole strategy is finally applied on a Duffing oscillator without optimization's constraint and a gantry crane to illustrate the efficiency on constrained optimization. In addition, many discussions are made relative to the number of initial sample points. The results show that the proposed approach is able to find the global optimum with a limited number of solver calls, demonstrating its ability to be integrated into an actual industrial design process.

Keywords: Constrained global optimization – Nonlinear Vibration – Bayesian Optimization – Gaussian Process – Harmonic Balance Method – Duffing oscillator – Gantry crane

- Open Archive HAL with file: hal-04394206
- Doi: 10.1007/s00158-024-03747-5

Contents

1 Introduction

The design of complex mechanical structures is an essential process for which the optimal mechanical performance of the structures is pursued in order to satisfy challenging standards that are constantly evolving. However, this process faces a contradiction between the need for high-fidelity numerical simulations and the requirement for efficient optimization strategies. In the case of vibration dynamics, linear models are often insufficient to capture local nonlinear phenomena such as contact and friction, leading to the use of overly conservative safety margins [1]. One current important concern of industrial companies remains to reduce these margins. This is for example the case in processes such as industrial structures retrofitting or mass reduction, leading to enhancements in energy consumption and cost savings (see for instance [2]). Among numerous fields concerned by this issue, one can cite nuclear standards which have strongly evolved from the 2011 Fukushima accident [3, 4]. Another example is the transport industry which is facing the challenge of energy efficiency [5].

In order to contribute to addressing these issues, this work aims at proposing an efficient global strategy to pursue constrained global parametric optimizations on nonlinear structural mechanical problems on vibrations. As a way to provide an adapted framework for future uses of industrial solvers, the considered optimization process has to remain non-intrusive. The proposed approach addresses two arising challenges: (i) the seek for an efficient and robust mechanical solver that can deal with nonlinearities and underlying complicated phenomena (bifurcations, quasi-periodic oscillations, chaos, etc.), and (ii) the limitation of the number of expensive high-fidelity mechanical simulations. Thus, two main ingredients are introduced: (i) a mechanical nonlinear solver based on model order reduction using Hurty-Craig Bampton technique [6], Harmonic Balance Method (HBM) [7] and continuation technique, and (ii) a constrained Bayesian Optimizer [8].

The paper is organized as follows. First, a brief analysis of the previous works related to global parametric optimization of nonlinear dynamics problems is proposed (see Section 2). The considered optimization workflow is presented after. Then, the mechanical solver, relying on HBM, Alternating Frequency-Time (AFT) and a path-following continuation procedure, is detailed (see Section 3). Afterward, Bayesian Optimization (BO) is introduced (see Section 4). Gaussian Process (GP) models are briefly presented and the enrichment process using the Constrained Expected Improvement (CEI) is described and illustrated on academic mathematical problems (see Section 4.3). Finally, the whole strategy is applied for the unconstrained optimization of a Duffing oscillator (see Section 5.1) and the constrained optimization of an actual industrial gantry crane subjected to sporadic contact (see Section 5.2).

2 Previous works and considered approach

2.1 Nonlinear structural dynamics methods

In the context of nonlinear structure optimization in vibration dynamics, the quantities of interest for the evaluation of the objective and constraint functions (e.g. displacement, acceleration, resonance frequencies, mechanical stress, etc.) are obtained from the structure's steady-state response to an external excitation. For large industrial structures, the response is usually obtained through a finite element (FE) computation. Most of the time, industrial FE software products include nonlinear dynamical solvers generally based on a step-by-step time integration procedure such as the Newmark scheme [9–11]. These methods are however computationally costly, especially with weakly damped structures, since the computation of the transient response is required. Therefore, the use of one of these solvers in the context of global parametric optimization is not practicable.

More efficient methods have been developed and lately applied to industrial-scale problems. The shooting method [12–14] avoids the transient computation by seeking periodic solutions using the resolution of a boundary value problem. However, this technique requires numerous time integrations that can make it computationally expensive even though parallelization can be used. Methods based on orthogonal collocation [15] have been implemented in several software programs [16–20] but are not often used for large systems.

Finally, frequency domain methods, that aim at finding the Fourier coefficients of periodic solutions, have also been developed. Some studies use the trigonometric collocation [21, 22], but the HBM is the most widely used frequency domain method. First introduced as an analytical method [7, 23, 24], HBM has been improved over time, such as the incremental harmonic balance [25–28], making it suitable for numerical computation. The use of the alternating frequency-time domain method (AFT) [29] to evaluate the nonlinear terms in the time domain allows the consideration of a wide variety of nonlinearities. More recently, the use of HBM in combination with reduction techniques and continuation procedures [30] has led to applications on industrial-scale structures among which contact and friction problems for turbomachines [31–33], steam generators [34, 35], and spacecraft structures [36], but also nonlinear material problems with elastomeric isolators [37] for instance. Following these works, multiple software packages performing HBM have been proposed, some of which are listed in [38].

In conclusion, when looking for periodic solutions, HBM is an efficient, robust and suitable tool for the considered problem of local nonlinearities. Moreover, it is well adapted to be used as a parametric mechanical solver considered as *black-box* in an optimization procedure. It will be later described in detail in Section 3.

2.2 Structural mechanics optimization methods

Optimization techniques have been proved useful for the design of structures [39]. Most of the time, solvers are used as *black-box* to compute the objective and constraint functions. Since there is no explicit formulation of these functions with respect to the design variables, ensuring global minimum convergence remains an actual challenge because of lack of prior knowledge about local minima. Thus, a global optimization procedure is necessary. In this purpose, one strategy is to perform numerous local optimizations (e.g. gradient descent [40], quasi-Newton methods [41]) from different starting points. But there is no guarantee to find the global minimum and numerous function evaluations are needed. Other specific global optimization algorithms, often inspired by processes found in nature, have been developed such as simulated annealing [42], evolutionary methods [43], or swarm intelligence

[44, 45]. However, all of these methods require a significant amount of evaluations of the objective and constraint functions to converge accurately, and their use is not suitable for the optimization of large nonlinear structures.

More recently, surrogate-based optimization has been developed [46] to provide inexpensive accurate approximations of actual functions based on only a few evaluations of them. Consequently, it leads to significant reduction of the number of solver calls in various applications (optimization, sensitivity analysis, uncertainty quantification, etc.). It relies on the building of a machine-learning model able to approximate the *black-box* functions. Bayesian Optimization [8, 47–49] mixes surrogate models and the use of decision criterion (called *acquisition function*) for sequential selection and model updating. Several implementations have been proposed as listed in [49]. BO is generally based on Gaussian Process [50, 51] that is well adapted to the iterative process and provides robust error criterion along the design space.

Applications of optimization techniques on nonlinear mechanics problems in dynamics forms a wide field of research. The works of [52–54] focus on the use optimization to tune dynamic vibrations absorbers. Dedicated approaches for dealing with contact with and without friction have been presented in [55–58]. Consideration of topology optimization is currently also very active in the context of nonlinear structural mechanics, see for instance [59–67]. Optimization in the context of structural crashworthiness has been subject of many developments to improve efficiency of the whole process [63, 64, 68, 69]. Recently, a review presents optimization techniques dedicated to seismic structural design [70].

In order to avoid too expensive dynamical nonlinear problems, [60, 71–75] proposes the use of the Equivalent Static Load Method (ESLM). Readers can refer to [76] for a large review on optimization techniques for time-dependant problem.

Finally, Harmonic Balance Method (see Section 2.1), which is the chosen technique for solving mechanical problems along a frequency range, has been used in previous works on optimization. It has been employed with gradient descent [77, 78], or recently to serve the building and enrichment of a surrogate model in compliance with the definition of Bayesian Optimization [67, 79]. Another proposed approach [80] involves a Gaussian Process surrogate model built using nonlinear normal modes (NNM). NNM have been also used to achieve specified frequency-amplitude dependence [81]. Constrained optimization problems have been studied for the design of nonlinear energy sink using support vector machines [82].

In conclusion, although a very rich literature concerning optimization of nonlinear dynamics problems exists, the proposed strategy in this work is original in the sense that it aims at proposing a global constrained optimization strategy for nonlinear structures in vibration dynamics. The proposed work is incorporated in the context of the development of an efficient non-intrusive technique that could be applied to industrial-scale structures. For these reasons, the optimization is based in this work on the use of Bayesian Optimization using a Gaussian Process and a Constrained Expected Improvement acquisition function due to its ability to efficiently converge to the global minimum with a limited number of solver calls. Moreover, this strategy remains completely non-intrusive within the mechanical solver to be applied to industrial-scale structures.

2.3 Considered workflow

The whole developed optimization strategy is summarized on Fig. 1. The method relies on a Constrained Bayesian Optimization in combination with the Harmonic Balance Method and is referred to as *CBO-HBM* thereafter.

The mechanical solver (denoted *HBM solver* on Fig. 1) is employed to compute the structure's objective y and constraints h functions for a set of design parameters x. In the Bayesian Optimization framework, Gaussian Processes of the objective and constraint functions are built and iteratively enriched starting from an initial set of sample points $\mathrm{x}^{(i)}$, $i \in [\![1; n_\mathrm{s}]\!]$ and their associated responses. The enrichment procedure is governed by a Constrained Expected Improvement acquisition function α_{CEI}. For this purpose, an internal global common optimizer is used to select the best new candidate $\mathrm{x}^{(n_\mathrm{s}+j)}$ as enrichment point. Thus, at j-th iteration (denoted *BO iterations* on Fig. 1), the enrichment procedure based on an existing growing database of points and responses $\{\mathrm{x}^{(i)}, \mathrm{y}(\mathrm{x}^{(i)}), \mathrm{h}(\mathrm{x}^{(i)})\}$ with $i \in [\![1; n_\mathrm{s} + j]\!]$ is the key point of the Bayesian Optimization. Finally, a convergence criterion or a dedicated budget (allowed number of FEM simulations or computation time) is used to stop the Bayesian Optimization.

All these notions as well as the general workflow and the notations introduced in Fig. 1 are later detailed and discussed in Section 4.

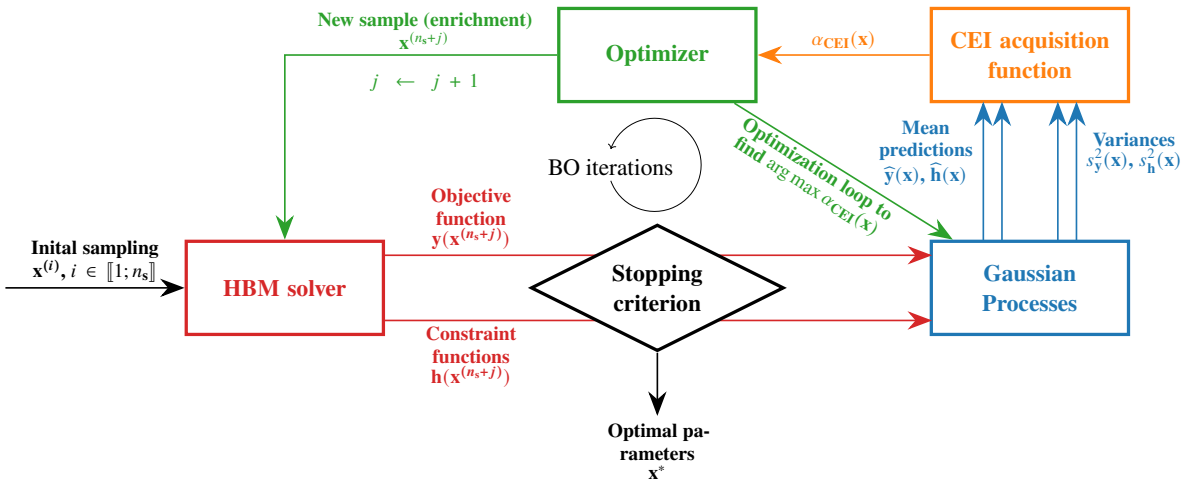

Figure 1: Workflow of the constrained optimization strategy.

Remark on the notations

The whole paper contains many specific notations for each part corresponding to different disciplines. Note that the bold style is used to designate vectors and matrices. In addition, lowercase bold notation is used for vectors while uppercase bold notation is used for matrices.

3 Mechanical solver

The motion of a nonautonomous nonlinear dynamical system discretized with n degrees of freedom (DOFs) can be described by the general equation:

$$\boldsymbol{M}\ddot{\boldsymbol{q}}(t) + \boldsymbol{C}\dot{\boldsymbol{q}}(t) + \boldsymbol{K}\boldsymbol{q}(t) + \boldsymbol{f}_{\text{nl}}(\dot{\boldsymbol{q}}(t), \boldsymbol{q}(t)) = \boldsymbol{f}_{\text{ext}}(\omega, t), \tag{1}$$

where $\boldsymbol{M}$, $\boldsymbol{C}$ and $\boldsymbol{K}$ are respectively the mass, damping and stiffness matrices. Vector $\boldsymbol{q}$ represents the DOFs and the notations $\dot{\bullet}$ and $\ddot{\bullet}$ refer to the successive derivatives with respect to time t. Thus, notations $\ddot{\boldsymbol{q}}(t)$ and $\dot{\boldsymbol{q}}(t)$ designate respectively the speed and acceleration. Vector $\boldsymbol{f}_{\text{nl}}(\dot{\boldsymbol{q}}(t), \boldsymbol{q}(t))$ contains the nonlinear forces and $\boldsymbol{f}_{\text{ext}}(\omega, t)$ corresponds to the periodic excitation forces with angular frequency ω. The resolution of Eq. (1) over an excitation frequency range is carried out using an in-house Python program based on the HBM. The main elements of the method are detailed in the following subsections.

3.1 Harmonic Balance Method

The HBM [7, 23–28] aims at finding a periodic solution with angular frequency ω of Eq. (1) approximated by a Fourier series truncated to the n_{h}-th harmonic:

$$\boldsymbol{q}(t) \simeq \boldsymbol{a_0} + \sum_{k=1}^{n_{\text{h}}} \left(\boldsymbol{a_k} \cos(k\omega t) + \boldsymbol{b_k} \sin(k\omega t)\right), \tag{2}$$

with $\boldsymbol{a_k}$ and $\boldsymbol{b_k}$ the vectors of the real Fourier coefficients respectively related to the cosine and sine terms that are the unknowns in the frequency domain. Equally, $\boldsymbol{f}_{\text{nl}}$ and $\boldsymbol{f}_{\text{ext}}$ are approximated by a truncated Fourier series where the vectors of the Fourier coefficients are respectively denoted $(\boldsymbol{a}_{\boldsymbol{k}}^{\text{nl}}, \boldsymbol{b}_{\boldsymbol{k}}^{\text{nl}})$ and $(\boldsymbol{a}_{\boldsymbol{k}}^{\text{ext}}, \boldsymbol{b}_{\boldsymbol{k}}^{\text{ext}})$:

$$\boldsymbol{f}_{\text{nl}}(\boldsymbol{q}(t), \dot{\boldsymbol{q}}(t)) \simeq \boldsymbol{a}_{\boldsymbol{0}}^{\text{nl}} + \sum_{k=1}^{n_{\text{h}}} \left(\boldsymbol{a}_{\boldsymbol{k}}^{\text{nl}} \cos(k\omega t) + \boldsymbol{b}_{\boldsymbol{k}}^{\text{nl}} \sin(k\omega t)\right), \tag{3}$$

$$\boldsymbol{f}_{\text{ext}}(\omega, t) \simeq \boldsymbol{a}_{\boldsymbol{0}}^{\text{ext}} + \sum_{k=1}^{n_{\text{h}}} \left(\boldsymbol{a}_{\boldsymbol{k}}^{\text{ext}} \cos(k\omega t) + \boldsymbol{b}_{\boldsymbol{k}}^{\text{ext}} \sin(k\omega t) \right). \tag{4}$$

The following frequency variables are then introduced to gather these coefficients into $n(2n_{\text{h}}+1) \times 1$ vectors:

$$\widetilde{\boldsymbol{q}} = \begin{bmatrix} \boldsymbol{a}_{\boldsymbol{0}}^{\top} & \boldsymbol{a}_{\boldsymbol{1}}{}^{\top} & \boldsymbol{b}_{\boldsymbol{1}}{}^{\top} & \cdots & \boldsymbol{a}_{\boldsymbol{k}}^{\top} & \boldsymbol{b}_{\boldsymbol{k}}^{\top} & \cdots & \boldsymbol{a}_{\boldsymbol{n}_{\text{h}}}{}^{\top} & \boldsymbol{b}_{\boldsymbol{n}_{\text{h}}}{}^{\top} \end{bmatrix}^{\top}, \tag{5}$$

$$\widetilde{\boldsymbol{f}}_{\text{nl}} = \begin{bmatrix} \boldsymbol{a}_{\boldsymbol{0}}^{\text{nl}\top} & \boldsymbol{a}_{\boldsymbol{1}}^{\text{nl}\top} & \boldsymbol{b}_{\boldsymbol{1}}^{\text{nl}\top} & \cdots & \boldsymbol{a}_{\boldsymbol{k}}^{\text{nl}\top} & \boldsymbol{b}_{\boldsymbol{k}}^{\text{nl}\top} & \cdots & \boldsymbol{a}_{\boldsymbol{n}_{\text{h}}}^{\text{nl}\top} & \boldsymbol{b}_{\boldsymbol{n}_{\text{h}}}^{\text{nl}\top} \end{bmatrix}^{\top}, \tag{6}$$

$$\widetilde{\boldsymbol{f}}_{\text{ext}} = \begin{bmatrix} \boldsymbol{a}_{\boldsymbol{0}}^{\text{ext}\top} & \boldsymbol{a}_{\boldsymbol{1}}^{\text{ext}\top} & \boldsymbol{b}_{\boldsymbol{1}}^{\text{ext}\top} & \cdots & \boldsymbol{a}_{\boldsymbol{k}}^{\text{ext}\top} & \boldsymbol{b}_{\boldsymbol{k}}^{\text{ext}\top} & \cdots & \boldsymbol{a}_{\boldsymbol{n}_{\text{h}}}^{\text{ext}\top} & \boldsymbol{b}_{\boldsymbol{n}_{\text{h}}}^{\text{ext}\top} \end{bmatrix}^{\top}. \tag{7}$$

Eqs. (2) to (4) are substituted into Eq. (1) and the resulting expression is projected on the trigonometric basis following a Galerkin procedure [83] to get rid of the time dependency. This results in a $n(2n_{\text{h}}+1)$ nonlinear algebraic system:

$$\widetilde{\boldsymbol{r}}(\widetilde{\boldsymbol{q}}, \omega) = \boldsymbol{Z}(\omega)\, \widetilde{\boldsymbol{q}} + \widetilde{\boldsymbol{f}}_{\text{nl}}(\widetilde{\boldsymbol{q}}, \omega) - \widetilde{\boldsymbol{f}}_{\text{ext}}(\omega) = \boldsymbol{0}. \tag{8}$$

Using the symbol $\otimes$ to represent the Kronecker product, the $n(2n_{\text{h}}+1) \times n(2n_{\text{h}}+1)$ block diagonal matrix $\boldsymbol{Z}(\omega)$ writes:

$$\boldsymbol{Z}(\omega) = \omega^2 \boldsymbol{\nabla}^2 \otimes \boldsymbol{M} + \omega \boldsymbol{\nabla} \otimes \boldsymbol{C} + \boldsymbol{I}_{2n_{\text{h}}+1} \otimes \boldsymbol{K}, \tag{9}$$

where $\boldsymbol{I}_{2n_{\text{h}}+1}$ is the identity matrix of size $2n_{\text{h}}+1$ and $\boldsymbol{\nabla}$ is the differential operator defined by:

$$\boldsymbol{\nabla} = \begin{bmatrix} 0 & & & & \\ & \boldsymbol{\nabla_1} & & (0) & \\ & & \ddots & & \\ & & & \boldsymbol{\nabla_k} & \\ & & & & \ddots \\ & (0) & & & \boldsymbol{\nabla_{n_{\text{h}}}} \end{bmatrix}, \tag{10}$$

with:

$$\boldsymbol{\nabla_k} = \begin{bmatrix} 0 & k \\ -k & 0 \end{bmatrix}. \tag{11}$$

In the case of forced base motion, which is the situation in the case studied in Section 5.2, the terms related to the forced DOFs are separated and Eq. (8) is solved on the unknown DOFs.

The nonlinear Eq. (8) can be solved using an iterative procedure such as the Newton-Raphson method [84], employed in this work. Since the external force $\boldsymbol{f}_{\text{ext}}$ is known in the time domain and periodic, the determination of $\widetilde{\boldsymbol{f}}_{\text{ext}}$ is straightforward. However, an analytical expression of the nonlinear forces is often not known in the frequency domain making the evaluation of the $\widetilde{\boldsymbol{f}}_{\text{nl}}$ term challenging.

3.2 The Alternating Frequency/Time method

The AFT algorithm introduced in [29] offers an efficient way to numerically compute the $\widetilde{\boldsymbol{f}}_{\text{nl}}$ term with successive transitions between the frequency and time domains using the discrete Fourier transform. The process is represented in Fig. 2 where the application of the direct discrete Fourier transform (DFT) is represented by the function $\mathscr{F}$ while the inverse discrete Fourier transform (DFT^{-1}) is denoted $\mathscr{F}^{-1}$. In this illustration, an arbitrary set of Fourier coefficients is taken for $\widetilde{\boldsymbol{q}}$, and the nonlinear term is such that $\boldsymbol{f}_{\text{nl}}(\dot{\boldsymbol{q}}(t), \boldsymbol{q}(t)) = 0.2\boldsymbol{q}^3(t)$.

Starting from the $\widetilde{\boldsymbol{q}}$ term, DFT^{-1} allows an evaluation of vectors $\boldsymbol{q}$ and $\dot{\boldsymbol{q}}$ at n_t time steps $(t_1, \cdots, t_{n_t})$ equally spread over a period:

$$\mathfrak{q} = \begin{bmatrix} \boldsymbol{q}(t_1) \\ \vdots \\ \boldsymbol{q}(t_{n_t}) \end{bmatrix} = \mathscr{F}^{-1}(\widetilde{\boldsymbol{q}}), \tag{12}$$

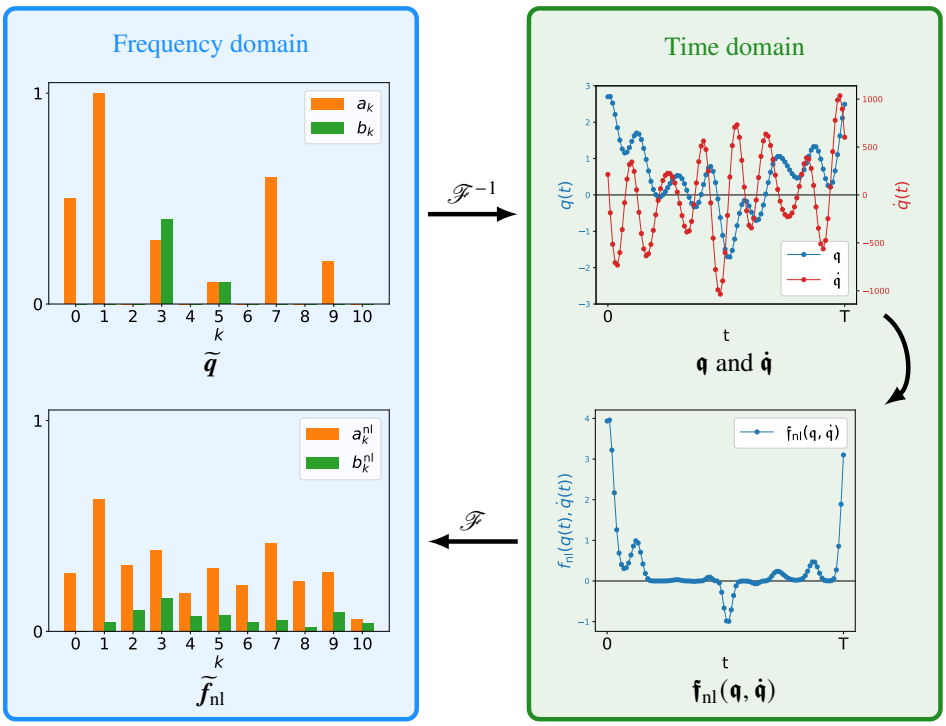

Figure 2: The alternating frequency time process.

$$\dot{\mathbf{q}} = \begin{bmatrix} \dot{\boldsymbol{q}}(t_1) \\ \vdots \\ \dot{\boldsymbol{q}}(t_{n_t}) \end{bmatrix} = \mathscr{F}^{-1}(\omega \boldsymbol{\nabla} \widetilde{\boldsymbol{q}}). \tag{13}$$

Assuming its analytical expression is known in the time domain, the nonlinear term is then evaluated at these time steps forming the $\mathbf{f}_{\text{nl}}$ vector written as:

$$\mathbf{f}_{\text{nl}}(\mathbf{q}, \dot{\mathbf{q}}) = \begin{bmatrix} \boldsymbol{f}_{\text{nl}}(\boldsymbol{q}(t_1), \dot{\boldsymbol{q}}(t_1)) \\ \vdots \\ \boldsymbol{f}_{\text{nl}}(\boldsymbol{q}(t_{n_t}), \dot{\boldsymbol{q}}(t_{n_t})) \end{bmatrix}. \tag{14}$$

The application of the DFT to this vector allows switching back to the frequency domain in order to obtain the $\widetilde{\boldsymbol{f}}_{\text{nl}}$ term. The whole process can be summarized by the following expression:

$$\widetilde{\boldsymbol{f}}_{\text{nl}}(\widetilde{\boldsymbol{q}}, \omega) = \mathscr{F}(\mathbf{f}_{\text{nl}}(\mathscr{F}^{-1}(\widetilde{\boldsymbol{q}}), \mathscr{F}^{-1}(\omega \boldsymbol{\nabla} \widetilde{\boldsymbol{q}}))). \tag{15}$$

The number of time steps n_t is a significant parameter here. In order to prevent aliasing errors, the Nyquist-Shanon criterion [85] gives a lower bound value: $n_t > 2n_{\text{h}}$, but a much larger value of n_t is often required to give an accurate estimation of the nonlinear term for strong nonlinearities. Although empirical rules depending on the mechanical system have been attempted, no global theory seems to exist to identify a correct number of samples [86].

The AFT technique therefore enables the resolution of Eq. (8) with a large variety of nonlinearities. Although the computational cost can be important with large values of n_t, the DFT can be performed efficiently using the *Fast Fourier Transform* (FFT) algorithm [87] making it computationally practicable. Moreover, the AFT method provides a semi-analytical expression of the residual's Jacobian presented on Eq. (8) needed for an iterative resolution (see [88–90] for details). This saves an important amount of time compared to a numerical evaluation with finite differences for instance.

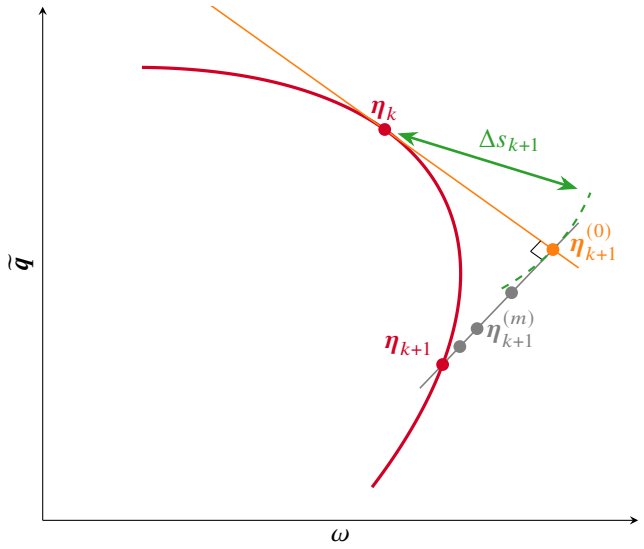

Figure 3: Schematic representation of the pseudo-arclength path continuation procedure in one dimension.

3.3 Path following continuation procedure

The previously mentioned Newton-Raphson iterative method to solve Eq. (8) requires an initial guess $\widetilde{\boldsymbol{q}}^{(0)}$. If this initial guess is not close enough to the exact solution, the convergence may be too slow or the solver may outright diverge. In this work, the values of the objective and constraint functions are obtained through the computation of the solution under the variation of the angular frequency excitation ω, called the frequency response. Since nonlinear dynamical systems exhibit complex behavior, bifurcations may occur and the Jacobian becomes singular at turning points, making impossible the iterative resolution. Numerical path following continuation has thus been applied with harmonic balance to compute a branch of solution points [91, 92]. This technique allows for overcoming turning points and increases the efficiency and robustness of the solver.

The predictor-corrector methods form a popular class of algorithms to perform continuation with the HBM [38, 93]. First, a prediction is made from the previously obtained solution. Corrections are then made using an iterative procedure with the prediction as an initial guess. Another alternative is based on the asymptotic numerical method [94, 95] and consists in expanding the solution path in a Taylor series with respect to an arc length parameter. In the present work, a predictor-corrector method is used since it is better suited for problems with strong nonlinearities such as unilateral contact [86]. The prediction is made with a tangent predictor and orthogonal corrections (sometimes referred as pseudo-arclength) are performed with the Newton-Raphson method.

In the following lines, the theory behind the pseudo-arclength path following continuation procedure is briefly explained. A schematic illustration of the process in 1D is given in Fig. 3.

Let $\boldsymbol{\eta}_k = \begin{bmatrix}\widetilde{\boldsymbol{q}}_k^\top & \omega_k\end{bmatrix}^\top$ be a previously found solution of Eq. (8). The unit tangent vector $\mathrm{t}_k = \begin{bmatrix}\mathrm{t}_{\widetilde{\boldsymbol{q}}_k}^\top & \mathrm{t}_{\omega_k}^\top\end{bmatrix}^\top$ is evaluated using the Keller algorithm [89, 96]. The predicted point $\boldsymbol{\eta}_{k+1}^{(0)}$ is taken on a hypersphere of Δs_{k+1} radius along the tangent vector:

$$\boldsymbol{\eta}_{k+1}^{(0)} = \boldsymbol{\eta}_k \pm \Delta s_{k+1} \mathrm{t}_k. \tag{16}$$

As detailed later, the prediction direction changes when fold bifurcations are encountered. The corrections are then iteratively made with the constraint that any next point must lie in the prediction direction orthogonal hyperplane. This results in the resolution of the following linear system to determine the increment $\Delta\boldsymbol{\eta}_{k+1}^{(m)} = \begin{bmatrix}\Delta\widetilde{\boldsymbol{q}}_{k+1}^{(m)} \\ \Delta\omega_{k+1}^{(m)}\end{bmatrix}$ at each iteration:

$$\begin{bmatrix}\boldsymbol{J}_{\widetilde{\boldsymbol{q}}}(\boldsymbol{\eta}_{k+1}^{(m)}) & \boldsymbol{J}_{\omega}(\boldsymbol{\eta}_{k+1}^{(m)}) \\ \mathrm{t}_{\widetilde{\boldsymbol{q}}_k} & \mathrm{t}_{\omega_k}\end{bmatrix}\begin{bmatrix}\Delta\widetilde{\boldsymbol{q}}_{k+1}^{(m)} \\ \Delta\omega_{k+1}^{(m)}\end{bmatrix} = \begin{bmatrix}\widetilde{\boldsymbol{r}}(\boldsymbol{\eta}_{k+1}^{(m)}) \\ 0\end{bmatrix}, \tag{17}$$

where $\boldsymbol{J}_{\widetilde{\boldsymbol{q}}}(\widetilde{\boldsymbol{q}},\omega) = \dfrac{\partial \widetilde{\boldsymbol{r}}}{\partial \widetilde{\boldsymbol{q}}}(\widetilde{\boldsymbol{q}},\omega)$ and $\boldsymbol{J}_{\omega}(\widetilde{\boldsymbol{q}},\omega) = \dfrac{\partial \widetilde{\boldsymbol{r}}}{\partial \omega}(\widetilde{\boldsymbol{q}},\omega)$ are the Jacobian matrices of $\widetilde{\boldsymbol{r}}$ with respect to $\widetilde{\boldsymbol{q}}$ and ω. The correction is reiterated as long as the norm of the residual $\|\widetilde{\boldsymbol{r}}\|$ is greater than a small fixed parameter ε.

In order to detect fold bifurcations, and thus the sign in Eq. (16), the test function defined in [97] is used. A fold bifurcation occurs when the Jacobian $\boldsymbol{J}_{\widetilde{\boldsymbol{q}}}$ has a single zero eigenvalue. The continuation method can then overcome turning point by ensuring that the sign in Eq. (16) is the same as the sign of $\det(\boldsymbol{J}_{\widetilde{\boldsymbol{q}}}(\boldsymbol{\eta}_k))$.

The step length Δs needs to be small enough to ensure fast convergence and to follow the nonlinear behaviors of the solution, but it should also be as large as possible to reduce the computational cost. It is common practice to automatically adapt Δs using empirical rules [38]. Many rules can be employed [92], but while working with Newton-type methods, the number of iterations until convergence is often used to adapt the step length [30]. In this work, the evolution of Δs is adapted from [90]:

$$\Delta s_{k+1} = \Delta s_k 2^{\frac{n_k^{\text{iter}} - n^{\text{tar}}}{n^{\text{tar}}}}, \tag{18}$$

with n_k^{iter} the number of iterations needed to compute $\boldsymbol{\eta}_k$ and n^{tar} a targeted number of iterations. A maximum and minimum value, respectively $\Delta s_{\max}$ and $\Delta s_{\min}$, are implemented. A maximum number of iterations $n_{\max}$ is also established, and if convergence is not achieved when this value is reached, the continuation process restarts with a smaller value for Δs (for instance, Δs can be divided by 2). Since no general rule exists, ε, n^{tar}, $\Delta s_{\min}$ and $\Delta s_{\max}$ are determined from empirical analysis depending on the studied structure. Another empirical trick used to improve the solver efficiency is to slightly increase Δs if $n_k^{\text{iter}} < n_{k-1}^{\text{iter}}$, even if $n_k^{\text{iter}} > n^{\text{tar}}$.

The association of the pseudo-arclength path following continuation procedure along with HBM and AFT is referred as the mechanical solver thereafter. It allows us to solve the nonlinear dynamical Eq. (1) over a range of frequencies.

4 Bayesian Optimization

During a parametric optimization process, the goal is to find the parameters x^* that minimize a particular quantity of interest, called objective function y. The mathematical expression of the unconstrained problem is:

$$\mathrm{x}^* = \underset{\mathrm{x}\in\mathcal{D}}{\arg\min}\, \mathrm{y}(\mathrm{x}), \tag{19}$$

where the design space $\mathcal{D}$ of dimension n_{p} denotes the design space of the varying parameters. But in a more general case, the parameters are subjected to a set of inequality constraints h_j for $j \in [\![1; r]\!]$, such that the constrained optimization problem is written:

$$\begin{aligned} \mathrm{x}^* = &\underset{\mathrm{x}\in\mathcal{D}}{\arg\min}\ \mathrm{y}(\mathrm{x}), \\ &\text{subjected to (s.t.) } \mathrm{h}_j(\mathrm{x}) \geq 0 \quad \forall j \in [\![1; r]\!]. \end{aligned} \tag{20}$$

The variation of y over $\mathcal{D}$ is typically unknown and local minima can exist. It is therefore required to conduct a global optimization procedure. Although the mechanical solver defined in Section 3 can be relatively efficient compared to other nonlinear dynamical solvers, it remains too expensive to be used within a usual global optimization algorithm [42–45] requiring many evaluations of the objective function (several hundred or even thousands). The proposed strategy, thus relies on a Bayesian Optimization [8, 47] based on Gaussian Process surrogate model approximating the objective and all the constraint functions. An acquisition function is used to iteratively enrich all the surrogate models. This optimization phase is here conducted using the Python library *BoTorch* [98] and the integrated GP model from *GPyTorch* [99] both built on the *PyTorch* module. Thereafter, a brief explanation of the theoretical background of GP and BO is given. For more details about the tackled notions, one can refer to [51, 100]. Finally, a short review on surrogate-based evolutionary optimization techniques can be found in [101].

4.1 Gaussian Process surrogate model

A surrogate model (or metamodel) is a mathematical model that aims at approximating a function from a limited number of analysis data. In engineering, they can be used to interpolate the results coming from an expensive

simulation, to act as calibration mechanisms for predictive codes, to deal with noisy or missing data or gain insight into the functional relationships between variables [102]. The literature on surrogate models is vast and numerous methods have been developed for the past 40 years. The range of use is also wide and leads to many reviews and comparisons of surrogate models applied to different fields. Especially, previous works aim at comparing surrogates for global approximation [103–114], optimization with surrogate models [115–132], uncertainty quantification [133, 134], multi-fidelity approaches [135], and sensitivity analysis [136]. Among these reviews, Gaussian Process [50] appears to be an efficient and robust surrogate model that can be used for a wide range of applications. Although it is not the most efficient surrogate model on certain applications, it can provide a robust error estimator based on a rigorous probabilistic framework which can be used within the acquisition function of a Bayesian Optimization.

In this work, the expensive objective and constrained functions y and h_j are approximated using independent GP surrogate models.

For simplicity's sake, the following paragraphs detail the theory behind GP for the approximation of y. Constraint functions are built using the same principle.

Gaussian Process prediction was first used in the geostatistical field by D. Krige [137] where the method is called *kriging* [138] and in meteorology [139]. It was applied in the context of computer experiments [140] based on deterministic observation data which inspired the Efficient Global Optimization (EGO) method presented by [8]. In this study, the functions are evaluated through a mechanical simulation which is considered deterministic. Therefore, all the surrogate models need to interpolate the data over the evaluated points.

The surrogate model of a function y is built from a set of n_s sample points $\mathrm{x}^{(i)} \in \mathcal{D}$ and the corresponding observations $\mathrm{y}(\mathrm{x}^{(i)})$ for $i \in [\![1; n_\mathrm{s}]\!]$. Throughout this work, the samples are determined using a Latin-Hypercube method [141] because it gives non-redundant sampling with a low discrepancy. The function y is supposed to be the fulfillment of a stochastic process Y described by its mean function μ and its kernel function (or covariance function) κ. For each $\mathrm{x} \in \mathcal{D}$, $Y(\mathrm{x})$ follows a normal distribution $\mathcal{N}(\mu(\mathrm{x}), \kappa(\mathrm{x}, \mathrm{x}))$ such that $Y(\mathrm{x}) = \mu(\mathrm{x}) + Z(\mathrm{x})$, with $Z(\mathrm{x})$ being a random variable that satisfies $\mathrm{cov}(Z(\mathrm{x}^{(i)}), Z(\mathrm{x}^{(j)})) = \kappa(\mathrm{x}^{(i)}, \mathrm{x}^{(j)})$ for $i,\ j \in [\![1; n_\mathrm{s}]\!]$. The mean function of Y is sought as a regression:

$$\mu(\mathrm{x}) = \sum_{m=1}^{p} \beta_m f_m(\mathrm{x}), \tag{21}$$

where $(f_m)_{m\in[\![1;p]\!]}$ are p basis functions (usually chosen polynomial) and $(\beta_m)_{m\in[\![1;p]\!]}$ are the associated coefficients of the regression. Moreover, this work uses the Matérn 5/2 kernel which is acknowledged as an efficient default kernel function [49]. For two observed parameters set $\mathrm{x}^{(i)}$ and $\mathrm{x}^{(j)}$, the kernel function then writes:

$$\kappa(\mathrm{x}^{(i)}, \mathrm{x}^{(j)}) = \sigma^2 \left(1 + \sqrt{5}d + \frac{5}{3}d^2\right) \exp(-\sqrt{5}d), \tag{22}$$

where $d = (\mathrm{x}^{(i)} - \mathrm{x}^{(j)})^\top \Theta^{-2} (\mathrm{x}^{(i)} - \mathrm{x}^{(j)})$ is the distance between $\mathrm{x}^{(i)}$ and $\mathrm{x}^{(j)}$ scaled by the lengthscale parameters matrix Θ, and σ is the standard deviation.

While fitting the GP with the n_s observations, the hyperparameters Θ, β_m and σ are determined by maximizing the likelihood of the sample using optimization methods. In this process, the vector $\boldsymbol{\beta} = (\beta_m)_{m\in[\![1;p]\!]}$ can be analytically expressed according to the other hyperparameters [50] :

$$\boldsymbol{\beta} = (\boldsymbol{F}^\top \boldsymbol{\mathcal{K}}^{-1} \boldsymbol{F})^{-1} \boldsymbol{F}^\top \boldsymbol{\mathcal{K}}^{-1} \boldsymbol{y}, \tag{23}$$

where for $(i, j) \in [\![1; n_\mathrm{s}]\!]$ and $m \in [\![1; p]\!]$:

- $\boldsymbol{F}$ is the matrix containing the regressors evaluated at the observation points such that $(\boldsymbol{F})_{mi} = f_m(\mathrm{x}^{(i)})$,
- $\boldsymbol{\mathcal{K}}$ is the symmetric kernel matrix such that $(\boldsymbol{\mathcal{K}})_{ij} = \kappa(\mathrm{x}^{(i)}, \mathrm{x}^{(j)})$,
- $\boldsymbol{y}$ is the observed responses vector such that $(\boldsymbol{y})_i = \mathrm{y}(\mathrm{x}^{(i)})$.

In this work, the hyperparameters are determined by maximizing the logarithm of the marginal likelihood using the *PyTorch* built-in Adam optimizer [142] with multiple restarts.

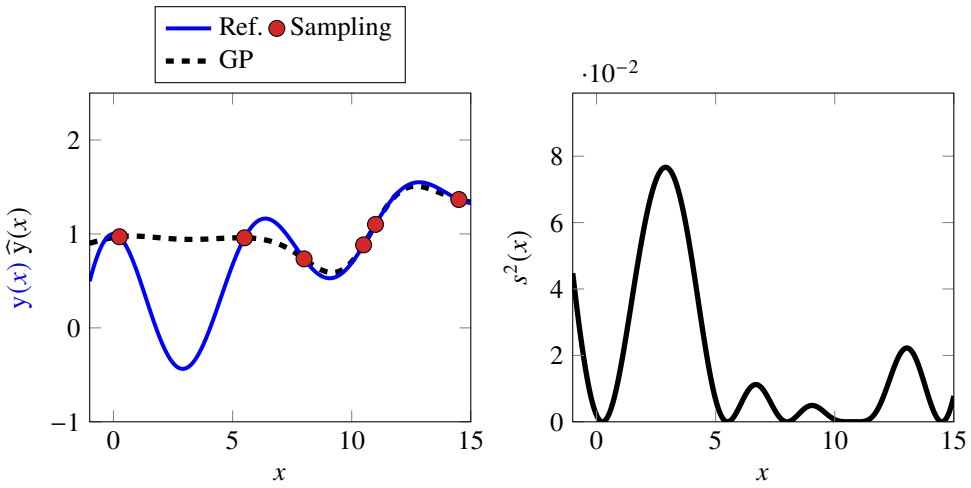

(a) Mean prediction. (b) Variance.

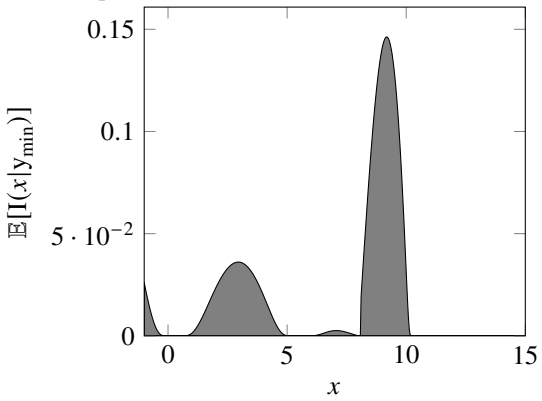

(c) Expected Improvement.

Figure 4: GP prediction for $\mathrm{y}(x) = \exp(-x/10)\cos(x) + x/10$ over $[-1;15]$.

To predict a point $\mathrm{x}^{(0)} \in \mathcal{D}$, the idea is to build the best linear unbiased predictor $\widehat{Y}(\mathrm{x}^{(0)})$ of the Gaussian Process $Y(\mathrm{x}^{(0)})$. This predictor provides a mean prediction $\widehat{\mathrm{y}}(\mathrm{x}^{(0)})$ and the associated variance $s^2(\mathrm{x}^{(0)})$:

$$\widehat{\mathrm{y}}(\mathrm{x}^{(0)}) = \boldsymbol{f}^{(0)\top}\boldsymbol{\beta} + \boldsymbol{\kappa}^{(0)\top}\boldsymbol{\mathcal{K}}^{-1}(\boldsymbol{y} - \boldsymbol{F}\boldsymbol{\beta}), \tag{24}$$

$$s^2(\mathrm{x}^{(0)}) = \kappa(\mathrm{x}^{(0)}, \mathrm{x}^{(0)}) - \begin{bmatrix}\boldsymbol{\kappa}^{(0)}\\ \boldsymbol{f}^{(0)}\end{bmatrix}^{\top}\begin{bmatrix}\boldsymbol{\mathcal{K}} & \boldsymbol{F}\\ \boldsymbol{F}^{\top} & \boldsymbol{0}\end{bmatrix}^{-1}\begin{bmatrix}\boldsymbol{\kappa}^{(0)}\\ \boldsymbol{f}^{(0)}\end{bmatrix}, \tag{25}$$

with $\boldsymbol{f}^{(0)}$ the vector containing the p terms $f_m(\mathrm{x}^{(0)})$ of the regression basis evaluated at $\mathrm{x}^{(0)}$ and $\boldsymbol{\kappa}^{(0)}$ the kernel vector such that $(\boldsymbol{\kappa}^{(0)})_i = \kappa(\mathrm{x}^{(i)}, \mathrm{x}^{(0)})$. An illustration is proposed in Fig. 4 where a GP, built from 6 sample points, approximates the unidimensional actual function y such that $\forall x \in \mathbb{R}$, $\mathrm{y}(x) = \exp(-x/10)\cos(x) + x/10$. On Fig. 4, Expected Improvement (see Eq. (26)) is also plotted. As previously mentioned, since the data are deterministic, the prediction interpolates the sample points and the variance is equal to 0 at these points. The maximum values of the variance are found where information is lacking, which in the deterministic case corresponds to the areas of the design space that are the furthest from a sample point.

The use of GP thus provides an efficient way to approximate the objective and constraint functions, and the procurement of the standard deviation indicates its variability. This information allows the implementation of an enrichment criterion (also designated as *acquisition function*) to perform a Bayesian Optimization.

4.2 Optimization

Once the surrogate models are built, a global optimization could be performed directly on the surrogate models because they provide an approximation of the functions along the design space with negligible time compared to the evaluation of the actual functions. However, if the sampling does not permit a sufficiently good approximation around the global minimum of the objective function, the optimization process could lead to an incorrect minimum. Consequently, without prior knowledge about the functions, dense sampling is required. The strategy here is to use the surrogate model to identify the areas where samples need to be added to avoid densification on the whole design space which would lead to a high number of evaluations of the approximated functions. The surrogate model is then enriched iteratively until convergence of the predicted global minimum. The $\mathrm{x}^{(n_\mathrm{s}+j)}$ notation is used to refer to the j-th point added to the initial sampling.

Multiple criteria, called acquisition functions, have been established to select the enrichment area [143]. The Expected Improvement (EI) [144], at the core of the EGO method [8], is used here for the unconstrained problem presented on Eq. (19) because it offers a satisfying trade-off between exploration (trying new points in unknown regions to discover new information) and exploitation (refining around the best values already found). Given Y, a Gaussian Process fitted on $n_\mathrm{s} + j$ samples, for each point $\mathrm{x}^{(0)} \in \mathcal{D}$ with predictor $\widehat{Y}(\mathrm{x}^{(0)})$, the EI acquisition function α_EI writes:

$$\begin{aligned}\alpha_\mathrm{EI}(\mathrm{x}^{(0)}) =& \mathbb{E}[\mathrm{I}(\mathrm{x}^{(0)}|\mathrm{y}_\mathrm{min})] \\ =& \left(\mathrm{y}_\mathrm{min} - \widehat{\mathrm{y}}(\mathrm{x}^{(0)})\right) \Phi(z(\mathrm{x}^{(0)})) + s(\mathrm{x}^{(0)})\phi(z(\mathrm{x}^{(0)})).\end{aligned} \tag{26}$$

The term $\mathrm{I}(\mathrm{x}^{(0)}|\mathrm{y}_\mathrm{min}) = \max(\mathrm{y}_\mathrm{min} - \widehat{Y}(\mathrm{x}^{(0)}); 0)$ is the potential for improvement over y_min, the minimum of y on the sampled points. The density probability and cumulative distribution function of the standard normal distribution are respectively denoted ϕ and Φ. The term z is such that $z(\mathrm{x}^{(0)}) = \dfrac{\mathrm{y}_\mathrm{min} - \widehat{\mathrm{y}}(\mathrm{x}^{(0)})}{s(\mathrm{x}^{(0)})}$. The next sample point is chosen to maximize the EI criterion:

$$\mathrm{x}^{(n_\mathrm{s}+j+1)} = \underset{\mathrm{x}^{(0)} \in \mathcal{D}}{\arg\max}\, \mathbb{E}[\mathrm{I}(\mathrm{x}^{(0)}|\mathrm{y}_\mathrm{min})]. \tag{27}$$

In the case of deterministic data, this acquisition function has the benefit to vanish at the sample points, avoiding adding samples too close to already observed points. The calculation of the expected improvement only involves the surrogate model and thus has a negligible computational cost. It is therefore possible to solve Eq. (27) computing the value of the EI on a fine mesh of the design space when its dimension is low enough, but an optimization algorithm is preferred for a higher number of parameters. However, the α_EI often has a lot of local minima which makes it difficult to find the actual global minimum. *BoTorch* directly integrates methods for the optimization of acquisition functions based on multi-start gradient descents. The determination of the initial sampling size requires careful consideration. An excessively high number of initial samples may lead to excessive computational costs, while too few samples could slow down or even obstruct the convergence of the strategy toward the global minimum. For the EGO algorithm, the choice of an initial sampling size around ten times the design space dimension ($n_\mathrm{s} = 10n_\mathrm{p}$) is recommended [8]. An illustration of this iterative process is given in Fig. 5 where the initial model built in Fig. 4 is enriched. On the first iteration, a sample is added near the predicted minimum which corresponds to a local minimum of the real function but not to the global minimum. On the second iteration, the enrichment is made where information is lacking, which proves the method's ability to explore the design space to find the global minimum. In the following iterations, the model is enriched to refine the predicted minimum and only a few iterations are needed to get an accurate estimation of the global minimum. Note that in Fig. 5, at each iteration, the Expected Improvement is plotted based on the new GP built using the new sample point (green diamond). The enriched sampling contains at each iteration the initial expanded with new (enriched) sample points from previous iterations.

In the case of constrained optimization of Eq. (19) (which only feature inequality constraints), the CEI [145, 146] is employed as an acquisition function. It consists in weighting the EI with the probabilities to satisfy the r inequality constraints $P(\mathrm{h}_j(\mathrm{x}^{(0)}) \geq 0)$. In the EI term, y_min is replaced by the best achievable value, denoted $\mathrm{y}^c_\mathrm{min}$, which corresponds to the minimum of y on the sampled points over the feasible region $\mathcal{A} = \{\mathrm{x}^{(0)} \in \mathcal{D} | \mathrm{h}_j(\mathrm{x}^{(0)}) \geq$

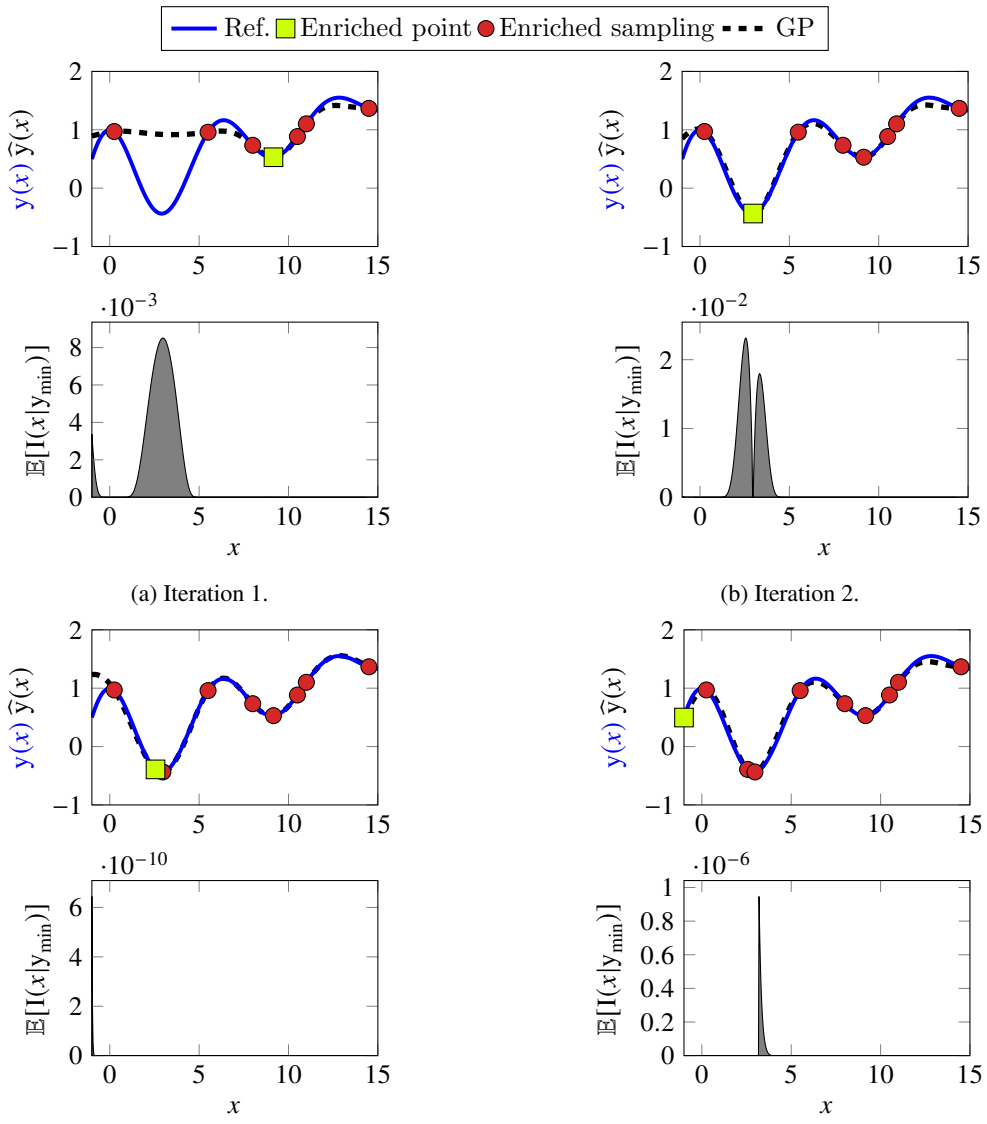

(a) Iteration 1.

(b) Iteration 2.

(c) Iteration 3.

(d) Iteration 4.

Figure 5: Enrichment illustration for $y(x) = \exp(-x/10)\cos(x) + x/10$.

0}. The expression of CEI acquisition function writes:

$$\alpha_{\mathrm{CEI}}(\mathrm{x}^{(0)}) = \mathbb{E}[\mathrm{I}(\mathrm{x}^{(0)}|\mathrm{y}^{c}_{\mathrm{min}})] \prod_{j=1}^{m} P(\mathrm{h}_j(\mathrm{x}^{(0)}) \geq 0). \tag{28}$$

To the knowledge of the authors, an extensive comparison of constrained global optimization algorithms, including variations of Bayesian optimization strategies, has not been published yet.

The stopping condition of the iterative enrichment process is often based on a budget: the algorithm stops when either a maximum number of solver calls is reached or a total computational time is exceeded. But other criteria based on the acquisition function values have been developed. One of them is used and detailed in Section 5.1.

The Bayesian Optimization approach allows a good approximation of the optimal parameters with a few costly evaluations of the objective function. If a precise optimum is needed, the optimization can be later refined using a local search around the solution reached [147, 148].

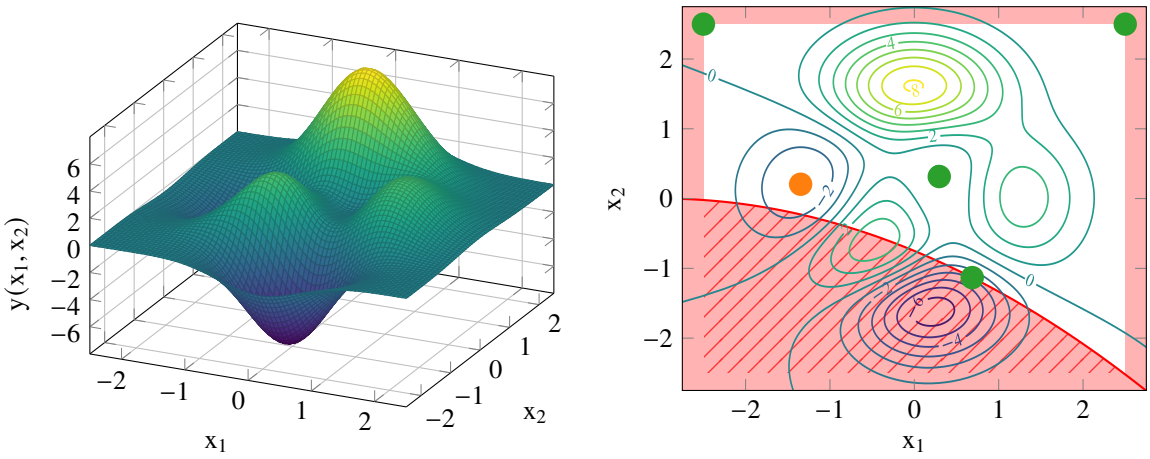

(a) Surface plot of the Peaks function.

(b) Contour plot of the Peaks function. The red hatched area represents the unfeasible domain under the constraint of Eq. (31). The orange dot (●) represents the location of the global minimum while the green dots (●) refers to the local minima.

Figure 6: Reference for the functions of the optimization problem on Eq. (30) over $\mathcal{D} = [-2.5; 2.5]^2$.

4.3 Example of application of the Constrained Bayesian Optimization

The constrained Bayesian Optimization approach is applied to find the minimum of the Peaks function from *Matlab*. The function is defined over $\mathcal{D} = [-2.5; 2.5]^2$ by:

$$\begin{aligned} y : \mathcal{D} &\to \mathbb{R} \\ (x_1, x_2) &\mapsto 3(1-x_1)^2 e^{-x_1^2-(x_2+1)^2} \\ &\quad - 10\left(\frac{x_1}{5} - {x_1}^3 - {x_2}^5\right) e^{-{x_1}^2-{x_2}^2} - \frac{1}{3} e^{-(x_1+1)^2-{x_2}^2}. \end{aligned} \tag{29}$$

The surface representation of the Peaks function is plotted on Fig. 6a. Multiple local minima exists which makes this example an interesting benchmark for optimization algorithms. The constrained optimization problem writes:

$$\begin{aligned} x^* = \quad & \underset{(x_1,x_2)\in[-2.5;2.5]^2}{\arg\min} && y(x_1, x_2), \\ & \text{s.t.} && h(x_1, x_2) \leq 0, \end{aligned} \tag{30}$$

with the constraint function defined by:

$$h(x_1, x_2) = -12x_2 - {x_1}^2 - 6x_1 - 9. \tag{31}$$

The contour plot of the Peaks function and the unfeasible domain are represented on Fig. 6b. The computation of the functions over a very fine mesh shows that problem on Eq. (30) admits a global minimum at $(-1.348; 0.205)$ with a reference value of -3.050. Problem on Eq. (30) also admits four local minima that are represented on Fig. 6b.

Several iterations of Eq. (30) solving process are depicted in Fig. 7. The surrogate models are initialized with 10 samples (Fig. 7a) and the enrichment process is repeated over 25 iterations. Until iteration 10 (Fig. 7c), points are mainly added around the local minima at (0.68,−1.13). At iteration 12 (Fig. 7d), the global minimum area is reached by the enrichment process. Finally, the last iterations are mainly dedicated to the exploitation in the global minimum region (Fig. 7e). This provides a fairly precise refinement of the obtained result. For a total of 35 evaluations of the objective function, the enrichment process results in a rather good approximation of critical

areas by the metamodel. Indeed, in addition to the exploitation around the global minimum, samples are added close to the local minima, which ensures there is no global minima in these locations. Numerous points are also present along the feasible domain boundary. The acquisition function representations show that α_{CEI} is strongly irregular, with a profusion of local minima. An important effort thus must be done to detect its global maximum. The evolution of the optimization process is depicted on Fig. 8. The best feasible minimum sampled y^c_{min}, and the maximum value of the acquisition function are represented with respect to n_y, denoting the number of objective (or constraint) function evaluations. In this example, the optimization strategy converges quickly towards the global minimum with a good accuracy. The acquisition function peak value globally decreases, but may exhibit local surges.

The resolution of the optimization problem on Eq. (30) is reproduced 30 times, for different number of initial samples, with a budget of 50 functions evaluations. The mean results are represented on Fig. 9. The optimization strategy is typically able to accurately find the global minimum after a few number of iterations for the largest numbers of initial samples ($n_s \geq 20$). It should however be noted that for some experiments, the enrichment process is not able to explore the whole domain and is still stuck around the local minimum after the 50 evaluations. This usually happens for small values of n_s when large areas of the design space are not covered by the initial sampling. This behavior is expected when optimizing challenging functions and is consistent with the results presented in [149]. Fig. 9b shows that the acquisition function maximum value globally decreases throughout the optimization process. A stopping criterion based on this quantity could then be considered in the case of constrained optimization.

The optimization strategy successfully accomplishes its primary objective of identifying the global minimum in a constrained optimization problem, requiring a reasonable number of function evaluations. The efficiency of the method is comparable with previous works on constrained Bayesian optimization [146, 150]. As highlighted in [49], a relatively small number of initial samples may lead to the best performances. The value $n_s = 10n_p$ remains a reliable choice in the constrained case to ensure a good convergence rate.

5 Application of the strategy

In the context of nonlinear dynamical structure optimization, the Bayesian Optimization process (Section 4) is implemented to find the optimal parameters of a mechanical problem whose objective and constraint functions are computed using the HBM solver (Section 3). The application of this whole *CBO-HBM* strategy whose workflow is represented in Fig. 1, is illustrated on two cases: an unconstrained and a constrained global optimizations respectively applied on a Duffing oscillator and a gantry crane.

5.1 Unconstrained optimization of a Duffing oscillator

In this section, the optimization strategy is applied for an unconstrained optimization problem on the Duffing oscillator inspired from [151]. The Duffing oscillator is a single degree of freedom system with cubic stiffness which makes it one of the simplest nonlinear mechanical system. This problem is studied because of its quite fast mechanical response computation (only 1 DOF). It allows to compute a reference objective function, which is interesting to follow the evolution of the enrichment process and to understand the behavior of the Expected Improvement acquisition function.

A schematic representation of the Duffing oscillator is given in Fig. 10a and its equation of motion writes:

$$m\ddot{q}(t) + \xi\dot{q}(t) + kq(t) + k_{\text{nl}}q^3(t) = f_e\cos(\omega t), \tag{32}$$

with m the mass, ξ the dumping factor, k the linear stiffness and k_{nl} the nonlinear stiffness. First introduced by Georg Duffing to study the large deflections of pendulums [152], this oscillator is a classical nonlinear problem and has been widely studied in the literature, for instance, in [153]. This system either softens, when $k_{\text{nl}} < 0$, or hardens, when $k_{\text{nl}} > 0$, throughout its motion. It can correspond to several mechanical or electrical systems. Despite its apparent simplicity, the Duffing oscillator can exhibit complex nonlinear phenomena such as period doubling bifurcations, quasi-periodic oscillations and even chaotic behavior. In this work, the system is only studied within a parameter range that allows a periodic solution having the same frequency as the excitation (the values are detailed later). Fig. 10b shows the maximum displacement of the Duffing oscillator for $\omega \in [0.05; 2.5]$

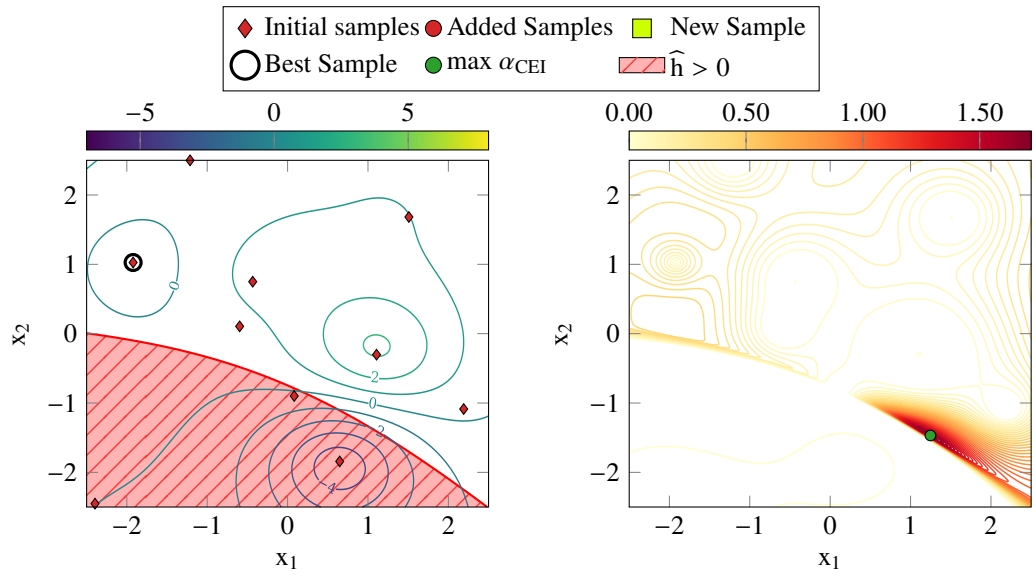

(a1) Predictions $\widehat{y}$ and $\widehat{h}$.

(a2) Acquisition Function α_{CEI}.

(a) Initialization.

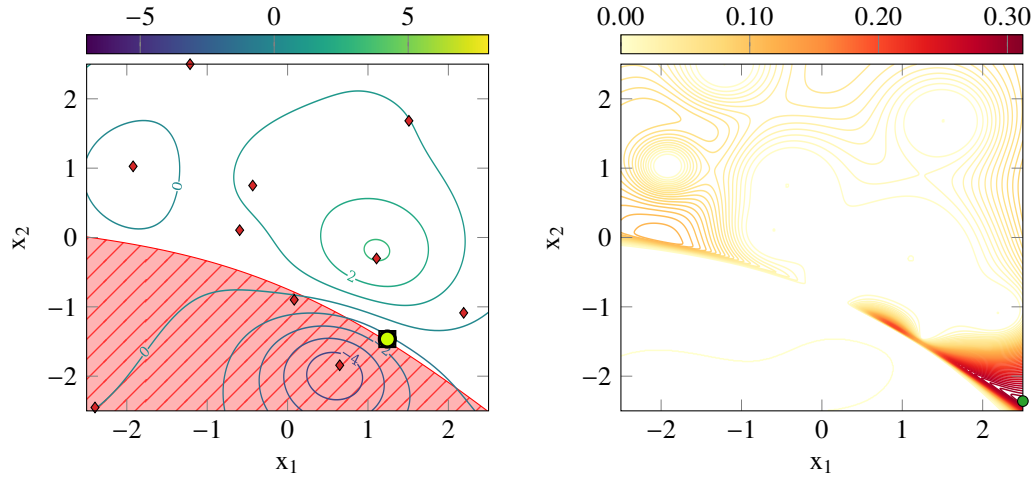

(b1) Predictions $\widehat{y}$ and $\widehat{h}$.

(b2) Acquisition Function α_{CEI}.

(b) Iteration 1.

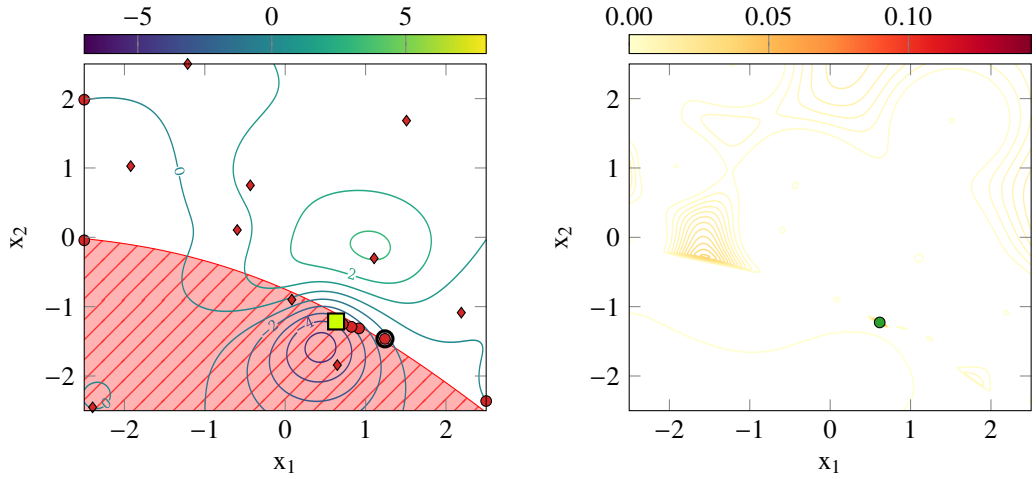

(c1) Predictions $\widehat{y}$ and $\widehat{h}$.

(c2) Acquisition Function α_{CEI}.

(c) Iteration 10.

Figure 7: Enrichment process to solve problem on Eq. (30) with 10 initial samples.

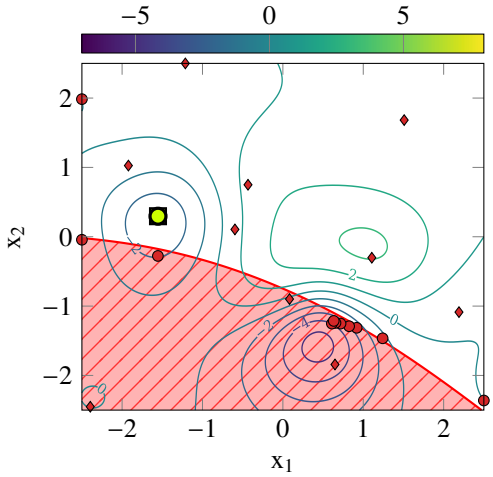

(d1) Predictions $\widehat{y}$ and $\widehat{h}$.

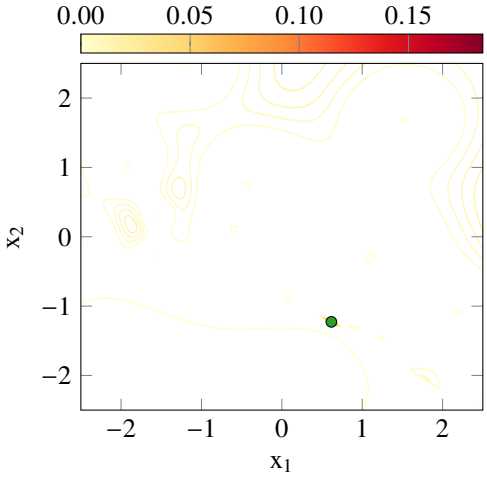

(d2) Acquisition Function α_{CEI}.

(d) Iteration 12.

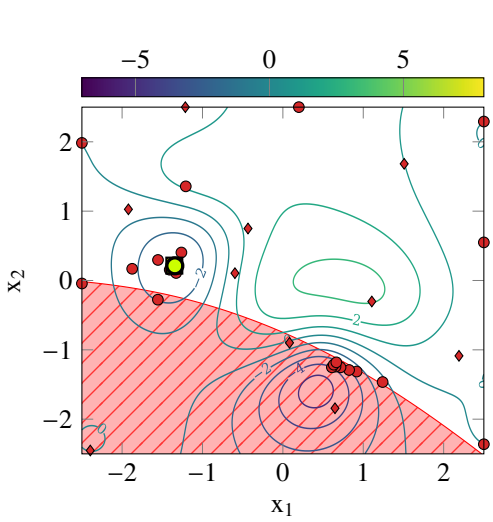

(e1) Predictions $\widehat{y}$ and $\widehat{h}$.

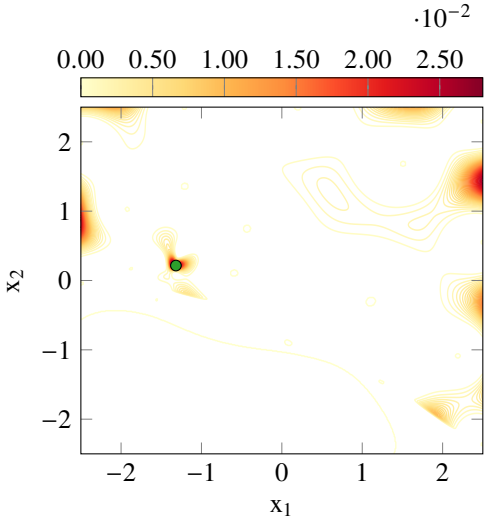

(e2) Acquisition Function α_{CEI}.

(e) Iteration 25.

Figure 7: Enrichment process to solve problem on Eq. (30) with 10 initial samples (cont.).

rad s^{-1} for several values of k_{nl} and illustrates the hardening or softening property of the system as well as the ability of the mechanical solver to overcome fold bifurcations.

The quantity of interest is the root-mean-square (RMS) of the acceleration, denoted $\ddot{q}_{\text{rms}}$. The two design parameters are the dumping factor ξ in the range $[0.1; 1]$ kg s^{-1} and the nonlinear stiffness k_{nl} in the range $[0.1; 2]$ N m^{-3} while the mass, the linear stiffness and the amplitude of the excitation are fixed: $k = 1$ N m^{-1}, $m = 1$ kg and $f_{\text{e}} = 0.3$ N. The RMS acceleration is calculated over a range of frequencies. No constraints are involved. The y objective function is taken as the maximum value reached by $\ddot{q}_{\text{rms}}$ for $\omega \in [0.05; 2.5]$ rad s^{-1}. The formulation of the optimization problem is:

$$(\xi^*, k_{\text{nl}}^*) = \underset{\substack{\xi \in [0.1;1]\,\text{kg s}^{-1} \\ k_{\text{nl}} \in [0.1;2]\,\text{N m}^{-3}}}{\arg\min} \; \text{y}(\xi, k_{\text{nl}}), \tag{33}$$

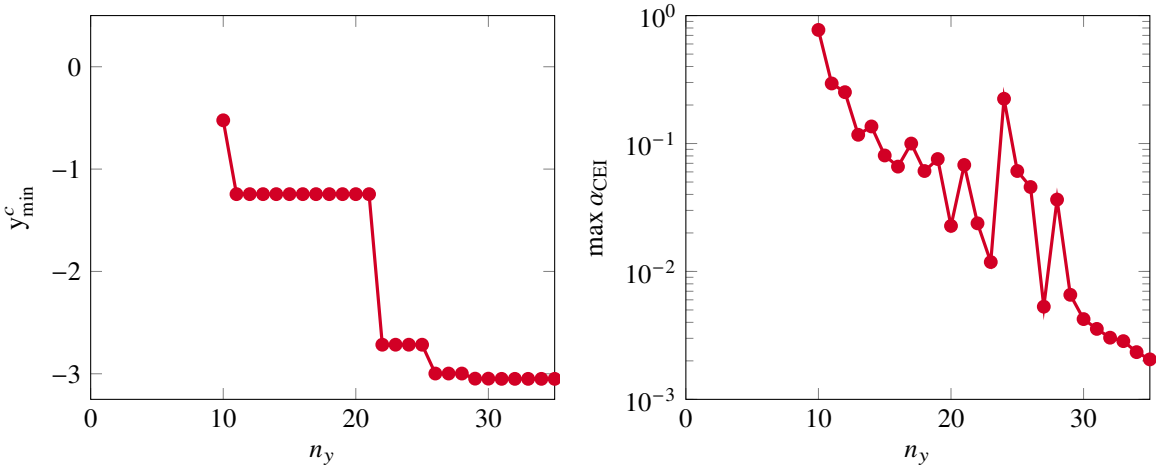

(a) Best feasible minimum evolution.

(b) Acquisition function evolution.

Figure 8: Best value and α_{CEI} peak value in relation to the objective and constraint functions evaluation count for the example shown on Fig. 7.

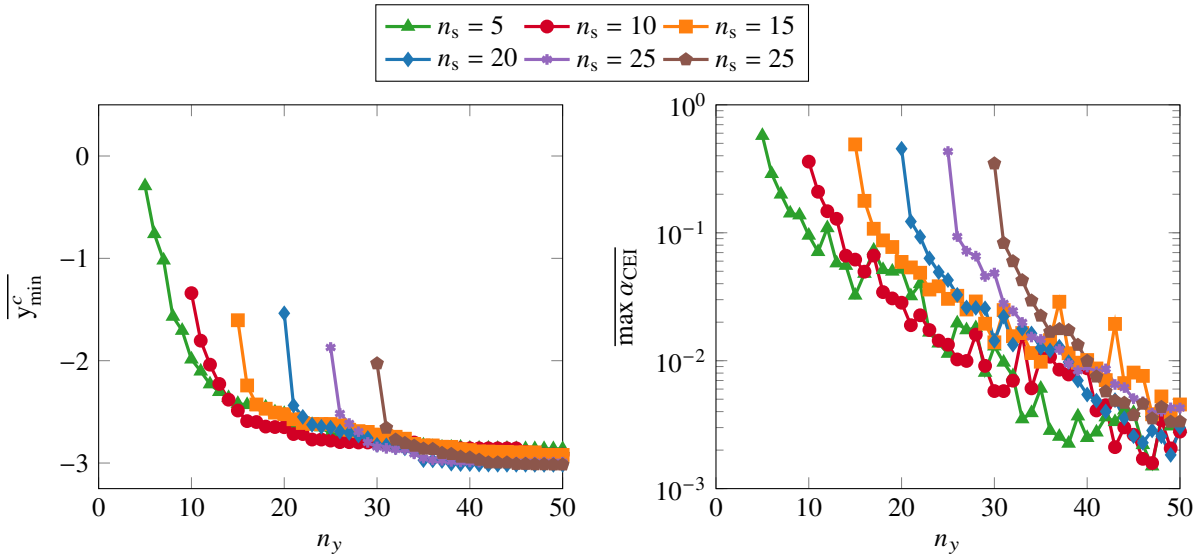

(a) Best feasible minimum mean values.

(b) Acquisition function mean values.

Figure 9: Mean values resulting from the repetition of 30 experiments for each number of initial samples.

with:

$$y(\xi, k_{nl}) = \max_{\omega \in [0.05;2.5]\,\mathrm{rad\,s^{-1}}} \ddot{q}_{rms}(\xi, k_{nl}, \omega). \tag{34}$$

For this unconstrained problem, the classic EI acquisition function is used (see Eq. (26)). The stopping criterion introduced in [8] is here examined. The algorithm stops once the ratio between the maximum value of the EI over $\mathcal{D}$ and $|y_{min}|$, called c_{EGO}, is less than a small parameter δ:

$$c_{EGO} = \max_{x^{(0)} \in \mathcal{D}} \frac{\mathbb{E}[I(x^{(0)}|y_{min})]}{|y_{min}|} < \delta. \tag{35}$$

A common choice for δ is 1% which is the employed value in this investigation.

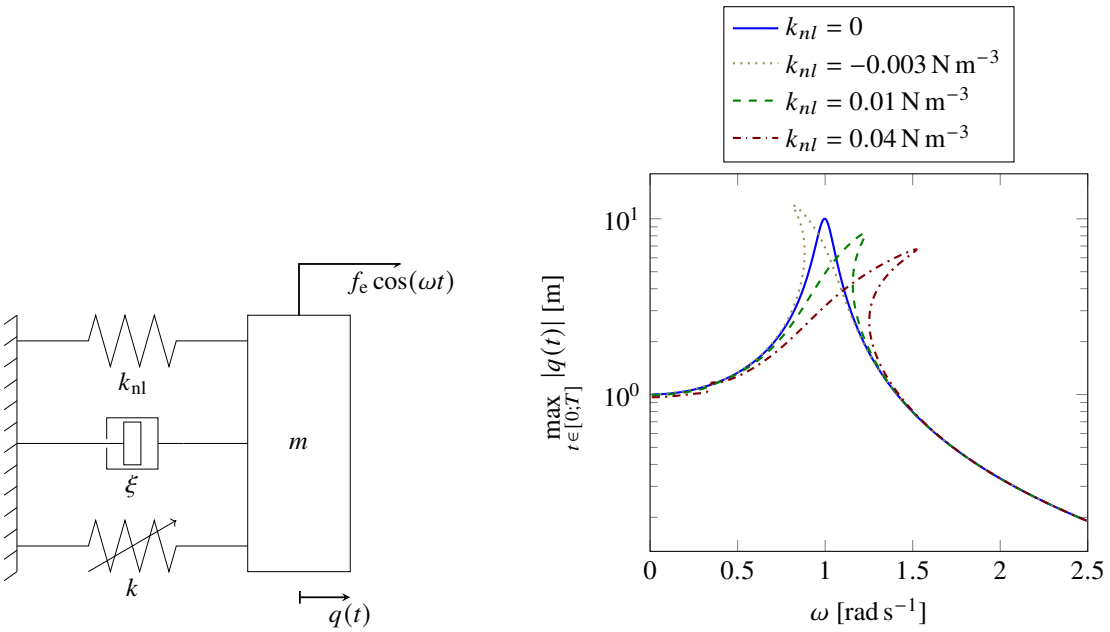

(a) Duffing oscillator representation.

(b) Maximum displacement amplitude of the Duffing oscillator along angular frequency (with $m = 1\,\mathrm{kg}$, $\xi = 0.1\,\mathrm{kg\,s^{-1}}$, $k = 1\,\mathrm{N\,m^{-1}}$, $f_e = 1\,\mathrm{N}$ and a few values of k_{nl}). HBM parameters: $n_h = 8$, $n_t = 40$, $\Delta s_{max} = 0.05$.

Figure 10: Duffing problem and frequency responses.

Figs. 11 and 12 show the evolution of $\ddot{q}_{rms}$ over $[0.05; 2.5]\,\mathrm{rad\,s^{-1}}$ for different sets of parameters. This result confirms the ability of the mechanical solver to solve Eq. (32) over the whole design space. It seems that the more k_{nl} increases, the more $\ddot{q}_{rms}$ increases and the more ξ increases, the more $\ddot{q}_{rms}$ reduces. The HBM parameters used here are: $n_h = 8$, $n_t = 40$, $\Delta s_{max} = 0.05$. These values remain the same throughout this section.

As only two parameters are involved in the optimization problem and the system only has 1 DOF, the objective function on Eq. (34) is computed over a fine mesh of the design space $\mathcal{D} = [0.1; 1] \times [0.1; 2]$ in order to use it as a reference and the result is represented in Fig. 13. This simulation confirms that $y(\xi, k_{nl})$ is minimal for $\xi = 1\,\mathrm{kg\,s^{-1}}$ and $k_{nl} = 0.1\,\mathrm{N/m^3}$. The evolution of the objective function is here quite simple, with no local minima. For this specific problem other methods such as local optimization algorithm [40] could probably be more efficient, but the goal of this study is to set up a robust enough strategy for any kind of optimization problems in nonlinear dynamics. It is nonetheless interesting to note that the objective function almost displays a plateau in some areas, which can be a hurdle to some methods, especially the gradient-based ones.

The optimization strategy is applied in the unconstrained case to solve problem presented on Eq. (33): a Bayesian Optimization is conducted relying on a Gaussian Process surrogate model which is built using the mechanical solver detailed in Section 3 to compute $\ddot{q}_{rms}$. A result of the whole process is presented in Fig. 14. The first surrogate model is computed with 15 initial samples (Fig. 14a). The stopping criterion on Eq. (35) is fulfilled after the addition of 33 points, totaling 48 calls to the mechanical solver. The enrichment process adds the global minimum point as early as the first iteration (Fig. 14b), but a substantial number of iterations ensue before the stopping criterion is met. This arises from the need to precisely approximate the plateau area, ensuring the absence of a lower minimum. This can be illustrated by the numerous samples added along the boundary $\xi = 1$ (Fig. 14d). Comparisons between Figs. 13 and 14d highlight the fact that the built surrogate model does not approximate accurately the objective function over the whole design space, but the enrichment process with the EI criterion is able to find and accurately estimate the area of the global minimum (unknown in the general case). For this problem, the computational cost of the EI acquisition function over a finely discretized mesh, spanning the whole design space, is sufficiently affordable to be illustrated in Fig. 14a, for all the iterations presented. This confirms

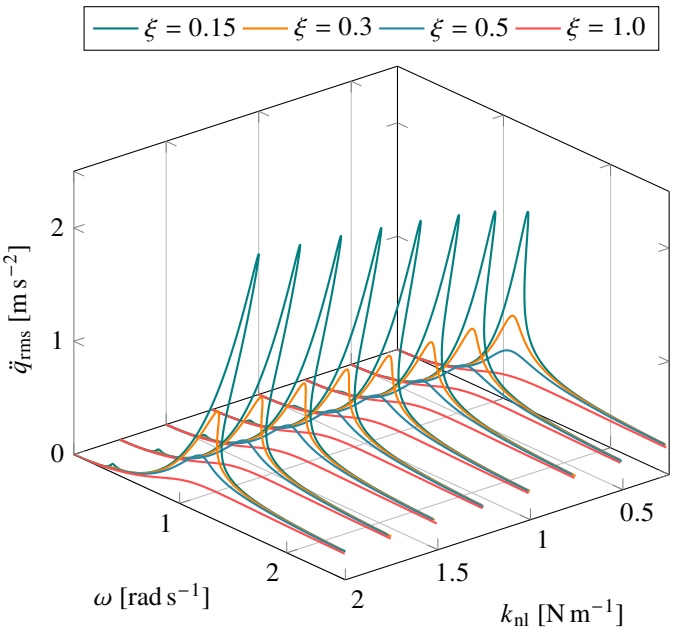

Figure 11: Frequency responses for a few pairs of values of ξ and k_{nl}.

Table 1: Objective function evaluations mean value using the stopping criterion $c_{\mathrm{EGO}} < 0.01$ for various numbers of initial samples n_{s}.

n_{s}	Iterations mean number	$\overline{n_y}$
10	35	45
15	47	62
20	59	79
25	58	83
30	59	89

that α_{EI} can have multiple local maxima and that the search for the global maximum may be challenging.

The optimization problem is reproduced 30 times with a different initial sampling to obtain an average number of requests to the mechanical solver. The process is repeated for different numbers of initial samples n_{s}, with a number of calls to the mechanical solver set to $n_y = 100$. The mean values and variances of the sampled minimum $\mathrm{y}_{\mathrm{min}}$ and the criterion c_{EGO} throughout the iterations are depicted in Fig. 15. The global minimum is consistently observed after only a few iterations of the enrichment process. However, as in the example presented in Fig. 14, c_{EGO} decreases gradually and quite slowly in all cases. The mean number of evaluations of the objective function to meet the criterion $c_{\mathrm{EGO}} > 0.01$ is summed up in Table 1. These results reveal that the smallest number of considered initial samples ($n_{\mathrm{s}} = 10$) yields the best performance, which aligns with the conclusions asserted in [49]. The relevance of the stopping criterion can however be questioned. On one hand, it leads to a seemingly excessive number of iterations for this specific problem, considering that the global minimum is accurately identified after only a few iterations. But on the other hand, this outcome could prove necessary to optimize functions characterized by multiple local minima surrounding a plateau.

This academic example of a Duffing oscillator optimization demonstrates the effectiveness of the presented strategy in solving a parametric optimization problem in nonlinear structural dynamics. The strategy achieves its primary goal by limiting the number of required calls to the mechanical solver.

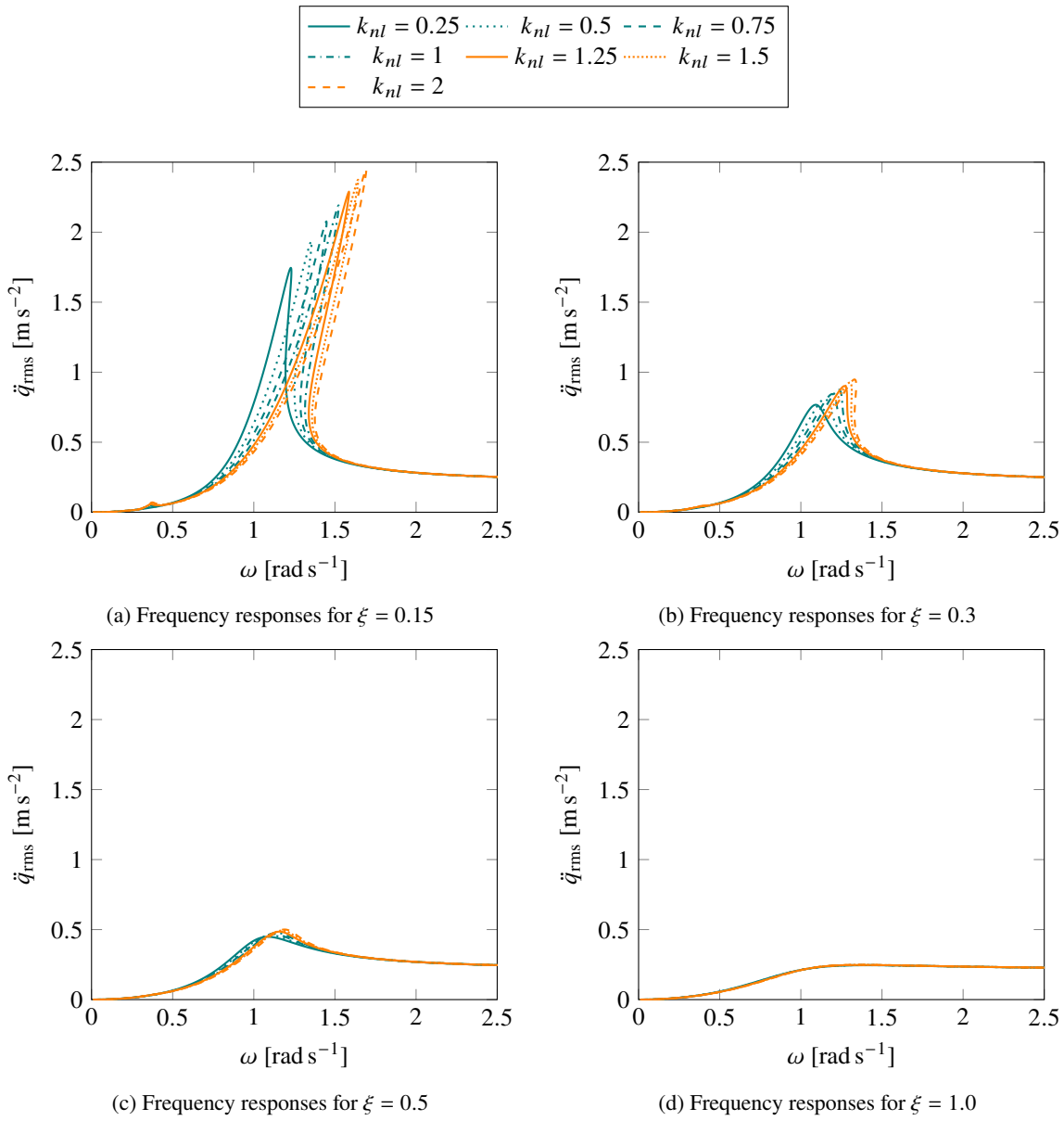

(a) Frequency responses for $\xi = 0.15$

(b) Frequency responses for $\xi = 0.3$

(c) Frequency responses for $\xi = 0.5$

(d) Frequency responses for $\xi = 1.0$

Figure 12: Parametric study of the Duffing oscillator. See also Fig. 11.

5.2 Constrained optimization of a gantry crane

To assess the *CBO-HBM* strategy on an industrial-scale, the optimal retrofit of a gantry crane is studied. Gantry cranes are industrial lifting devices intended to carry very heavy loads. The entire structure is wheeled (often on rails) and a trolley containing the hoist moves in a transversal direction. As these structures often operate in risky environments (e.g. nuclear sites) they need to satisfy demanding standards. One of the major issues is to prevent the overturning of the gantry when it is subjected to a base motion as it occurs during earthquakes.

5.2.1 Model description

During their lifetime, gantry cranes' designs may be required to be re-evaluated with more severe criteria, either due to an evolution of the standards or because they are used for a different program in another environment

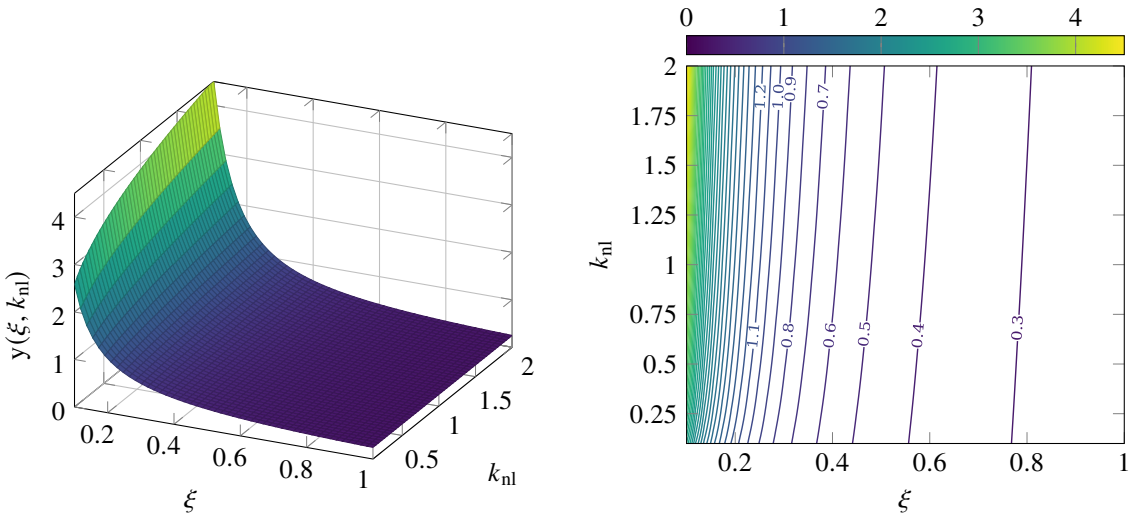

(a) Surface plot.

(b) Contour plot.

Figure 13: Reference for the objective function shown on Eq. (34).

[154]. Here, the retrofit of such a structure is studied with a focus on the optimal design of an anti-tipping device. The model of the structure is depicted in Fig. 16. The gantry is about 10 m high and 13 m wide with a payload of 65 t. The finite element model derives from an industrial study and the mesh convergence is ensured. The main parts of the structure are composed of 44 335 linear elastic steel shell elements and the bolted junctions are modeled using 302 bush elements. The model also contains 42 beam elements and 12 point mass elements to represent the wheels and their axles. In order to simplify the model and avoid accounting for the complex effects induced by a flexible cable, the payload is modeled by another point mass element at the center of the trolley. The analysis is therefore done under the assumption of small perturbations. The model has a total of 43 722 nodes, corresponding to around 260 000 DOFs. A schematic illustration of an anti-tipping device is given in Fig. 17. It consists of a beam, anchored to the ground, with the top end placed at an initial gap from a gantry leg to block its vertical displacement. With such a mechanism, two local contact phenomena can appear: after the detachment of the wheel, the gantry leg may reach the anti-tipping device and when the structure relapses, contact occurs with the ground (or the supporting rail). Throughout the motion, the structure's center of gravity velocity must be controlled to prevent overturning and the contact force on the anti-tipping device must be restrained enough to ensure the robustness of the anchor to concrete ground, which is the most critical.

As this problem is mainly intended as a proof of concept for the optimization strategy, some strong simplifications have been adopted on the mechanical model as shown in Fig. 18. Since most of the mass is concentrated at the center of the trolley, the transversal velocity is investigated at this point (point M), rather than at the actual center of gravity. The detachment of only one leg is studied: legs A, B and C are considered anchored to the ground and only leg D may suffer detachment and contact phenomena. The complex bogie at the end of that leg has been replaced by a single wheel modeled by a single node whose vertical translation DOF (denoted q_y^{D}) is subjected to contact. As represented in Fig. 18, the contact is accounted for using a penalty method: a k_2 stiffness value is added for the contact with the anti-tipping device with an initial gap written g and a k_1 stiffness value is added for the ground contact with no initial gap. The theoretical nonlinear force expresses:

$$F_c^{\mathrm{D}}(g, k_1, k_2) = \begin{cases} k_1 q_y^{\mathrm{D}} & \text{if} \quad q_y^{\mathrm{D}} \leq 0, \\ 0 & \text{if} \quad 0 < q_y^{\mathrm{D}} < g, \\ k_2(q_y^{\mathrm{D}} - g) & \text{if} \quad q_y^{\mathrm{D}} \geq g. \end{cases} \tag{36}$$

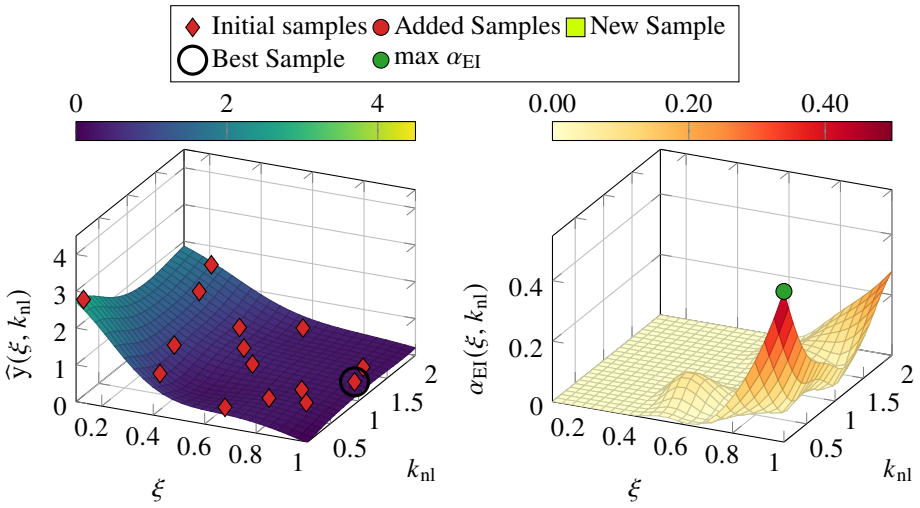

(a1) Prediction $\widehat{y}$.

(a2) Acquisition function α_{CEI}.

(a) Initialization.

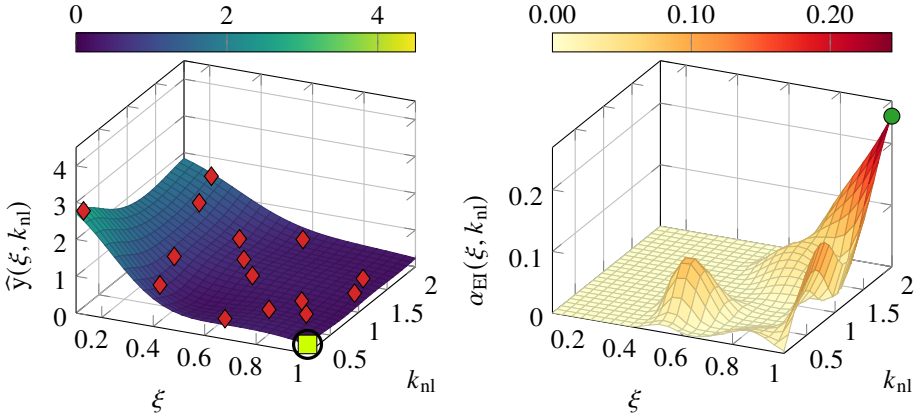

(b1) Prediction $\widehat{y}$.

(b2) Acquisition function α_{EI}.

(b) Iteration 1.

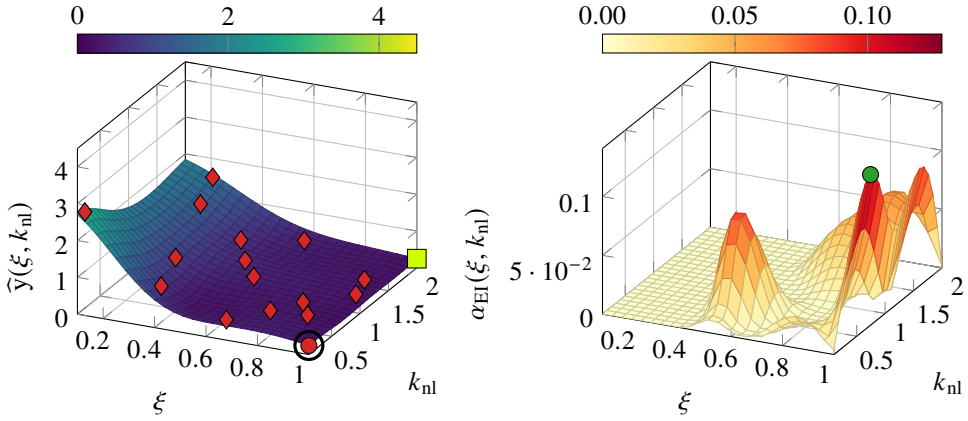

(c1) Prediction $\widehat{y}$. (c2) Acquisition function α_{EI}.

(c) Iteration 2.

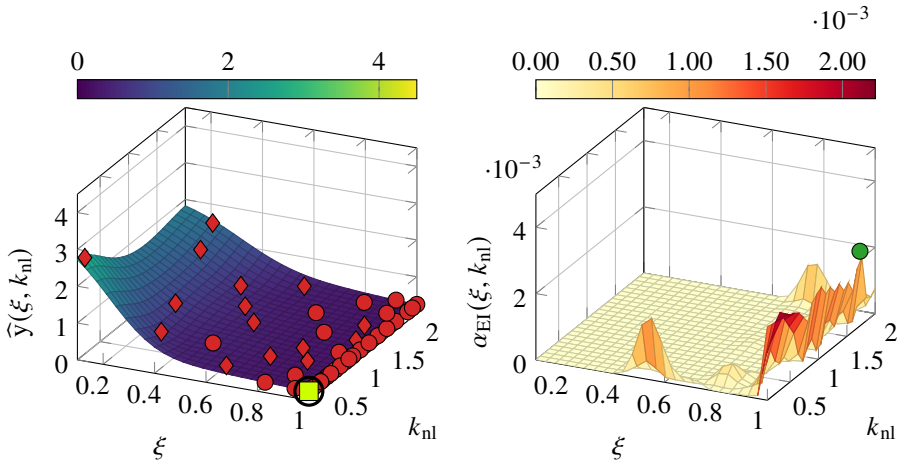

(d1) Prediction $\widehat{y}$. (d2) Acquisition function α_{EI}.

(d) Iteration 33 ($c_{EGO} < 0.01$).

Figure 14: Problem on Eq. (33) resolution with 15 initial samples.

To enhance the robustness of the mechanical solver, the contact law is smoothened as proposed on [90] such that:

$$F_c^D(g, k_1, k_2) = \frac{k_1 q_y^D}{2} - \sqrt{\left(\frac{k_1 q_y^D}{2}\right)^2 + \epsilon_1^2} + \frac{k_2(q_y^D - g)}{2} + \sqrt{\left(\frac{k_2(q_y^D - g)}{2}\right)^2 + \epsilon_2^2}, \tag{37}$$

with ϵ_1 and ϵ_2 additional parameters to adjust the smoothing of the contact law. A representation of this law is given in Fig. 19 with different values of these parameters. When $\epsilon_1 = \epsilon_2 = 0$, the regularized contact law on Eq. (37) is equivalent to the penalty method on Eq. (36). For the mechanical simulation of the gantry crane, the parameters have been fixed to $\epsilon_1 = 1 \times 10^2$ N and $\epsilon_2 = 1 \times 10^3$ N.

The structure undergoes a harmonic base motion with frequency within the typical seismic excitation range [0;35] Hz and whose acceleration magnitude, presented in Fig. 20, has been taken from the spectrums of randomly generated accelerograms in compliance with Eurocode 8 [155] standards for nuclear sites. The considered spectrum has a maximum constant value for low frequencies (between 1 Hz and 6 Hz) and slightly decreases for higher frequencies.

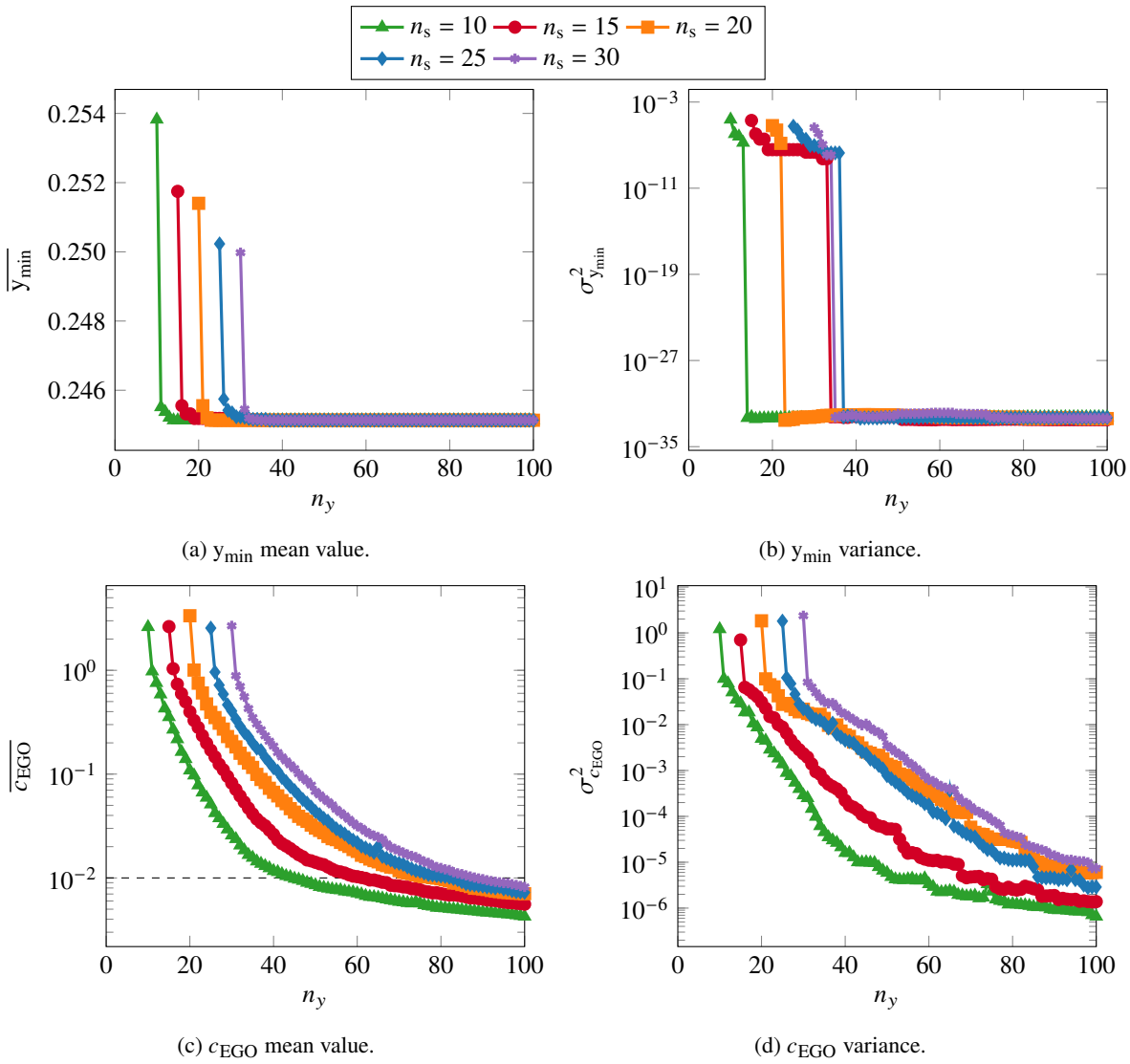

(a) y_{min} mean value.

(b) y_{min} variance.

(c) c_{EGO} mean value.

(d) c_{EGO} variance.

Figure 15: Repetition of 30 experiments in solving problem on Eq. (33) for various values of n_s with a budget fixed to $n_y = 100$.

5.2.2 Optimization problem

As previously stated, the quantity of interest sought to be minimized is the transversal velocity at point M, denoted v_T^M. A coarse analysis using *Hilti PROFIS Engineering* [156] software allowed us to determine that the limit value of the contact force ensuring the anti-tipping device anchor integrity under Eurocode 2 standards [157] is $F_{c\,\max}^D = 200\,\text{kN}$ which constitutes the constraint of the optimization problem. The contact stiffness between the wheel and the ground is set to $k_1 = 1 \times 10^7\,\text{N m}^{-1}$. The contact stiffness k_2 is a parameter of the optimization problem with values ranging from 0 to $1 \times 10^8\,\text{N m}^{-1}$. This can be influenced by the geometry and material of the anti-tipping device as well as the presence of elastomer patches to alleviate the contact. The other considered parameter here is the initial gap g with value varying between 5 mm (minimal practicable distance) and 40 mm (contact never occurring). To mathematically describe the problem, the parameters of the investigated optimization problem are:

$$\mathrm{x} = (g, k_2) \in \mathcal{D}, \tag{38}$$

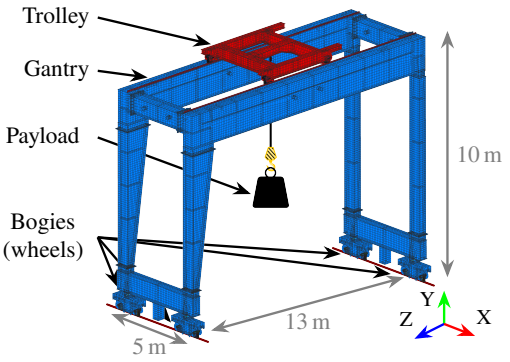

Figure 16: Model of the gantry crane.

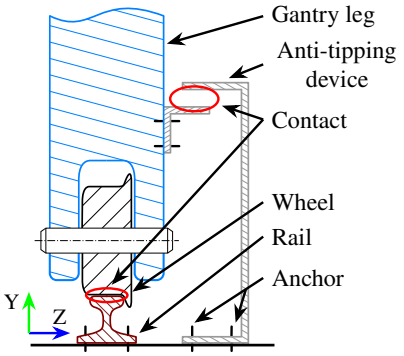

Figure 17: Illustration of an anti-tipping device.

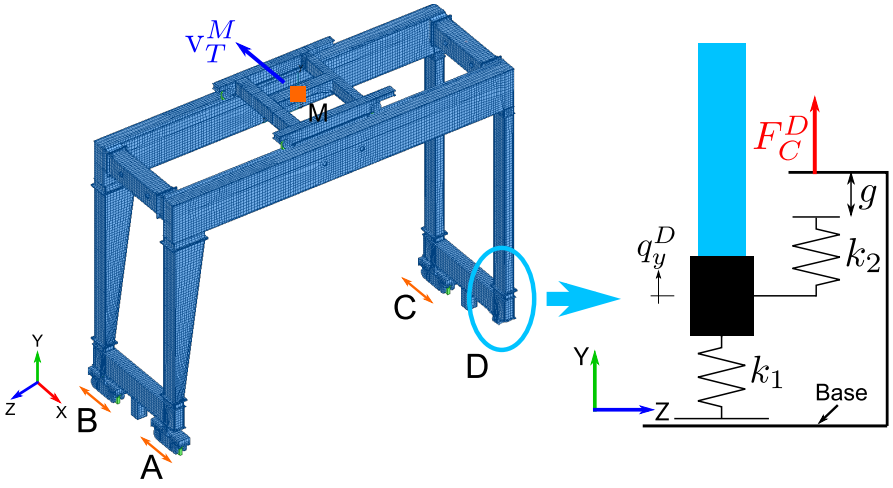

Figure 18: Simplified FE model: global FE mesh (left) and local simplified leg contact model (right).

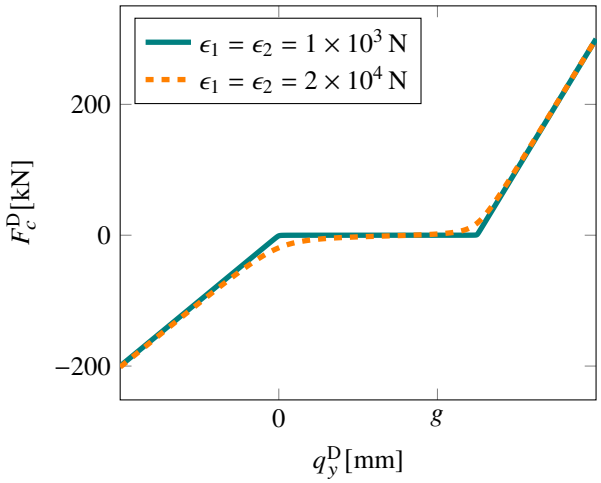

Figure 19: Representation of the contact force for $k_1 = 5{\times}10^7$ N m^{-1}, $k_2 = 1{\times}10^8$ N m^{-1}, $g = 4$ mm and different values of the smoothing parameters.

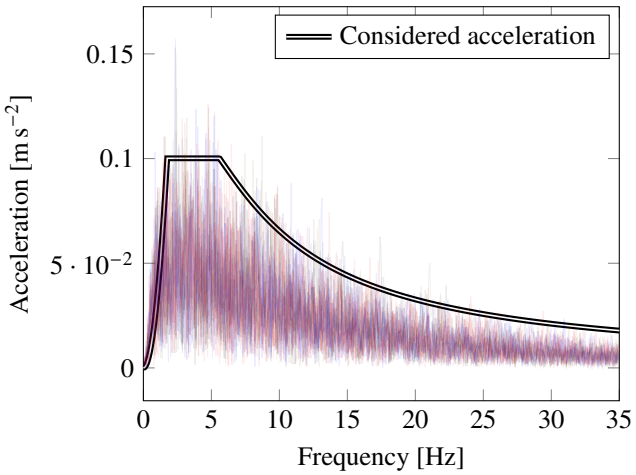

Figure 20: Base motion acceleration spectrum.

with the design space $\mathcal{D}$ such that:

$$\mathcal{D} = [5 \times 10^{-3}; 40 \times 10^{-3}] \times [0; 1 \times 10^{8}]. \tag{39}$$

The objective function is:

$$\mathrm{y}(g, k_2) = \max_{f \in [0;35]\ \mathrm{Hz}} v_T^{\mathrm{M}}(g, k_2, f), \tag{40}$$

and the constraint function writes:

$$\mathrm{h}(g, k_2) = \max_{f \in [0;35]\ \mathrm{Hz}} F_c^{\mathrm{D}}(g, k_2, f) - F_{c\ \max}^{\mathrm{D}}. \tag{41}$$

Finally, the constrained optimization problem is:

$$\begin{aligned} (g^*, k_2^*) = &\arg\min_{(g,k_2) \in \mathcal{D}} \mathrm{y}(g, k_2), \\ &\text{s.t. } \mathrm{h}(g, k_2) < 0. \end{aligned} \tag{42}$$

5.2.3 Mechanical simulation

In order to take advantage of the small number of nonlinear DOFs (only 1 in this considered simplified model), a Craig Bampton condensation [6] is applied. The reduced basis includes 24 interface DOFs and 87 condensed DOFs resulting in a total of 111 DOFs. As the DOF undergoing contact is among the interface DOFs, the nonlinear resulting force is not modified by the condensation. The mechanical solver specified in Section 3.1 is used to solve the reduced problem. Results are represented in Figs. 21a and 21b over a frequency range of [0;35] Hz for $g = 5\,\mathrm{mm}$ and $k_2 = 1 \times 10^8\,\mathrm{N\,m^{-1}}$ which is the case providing the strongest nonlinearities. The computation takes about 40 minutes and results in 649 frequency steps, with Δs adaptation providing smaller steps around the resonance peaks, which allows to correctly detect and follow the fold bifurcations. Figs. 21a and 21b show that only the first resonance peak may lead to contact with the anti-tipping device and have an influence on the objective and constraint functions. Therefore, during the optimization procedure, the solution will be only computed on the range [0;3] Hz to reduce the computational cost. The nonlinear effects are apparent in Figs. 21c and 21d where the frequency response is compared for the linear case (no contact at all)[1], the case with only ground contact and no contact with the anti-tipping device and finally the case represented in Figs. 21a and 21b with $g = 5\,\mathrm{mm}$ and $k_2 = 1 \times 10^8\,\mathrm{N\,m^{-1}}$. These results show that the ground contact leads to new resonance peaks (e.g. around 0.5 Hz and 1.95 Hz) and to an offset on the main resonance peak. The contact with the anti-tipping device is the source of a fold bifurcation and limits the vertical displacement q_y^{D}.

[1]The linear case is out of the scope of the present considered optimization problem, it is shown here to highlight the nonlinear effects.

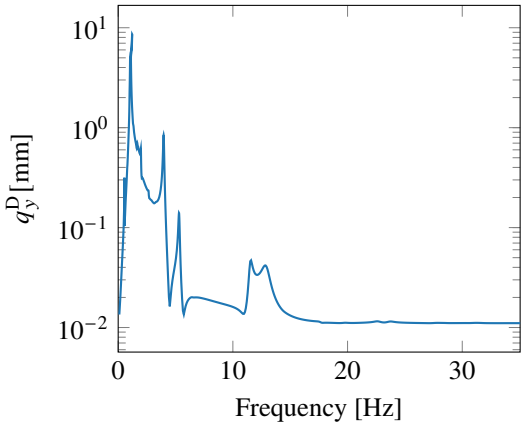

(a) Vertical displacement q_y^{D} for $g = 5\,\mathrm{mm}$ and $k_2 = 1 \times 10^8\,\mathrm{N\,m^{-1}}$.

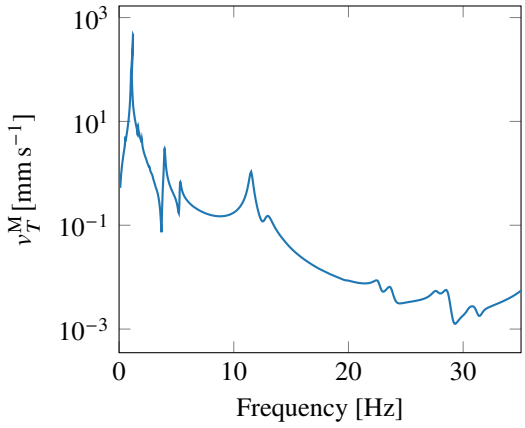

(b) Transversal velocity v_T^{M} for $g = 5\,\mathrm{mm}$ and $k_2 = 1 \times 10^8\,\mathrm{N\,m^{-1}}$.

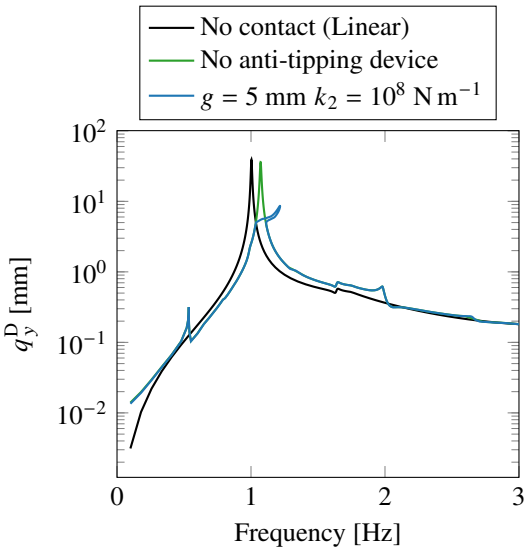

(c) Vertical displacement q_y^{D} on the reduced frequency bandwidth for different configurations.

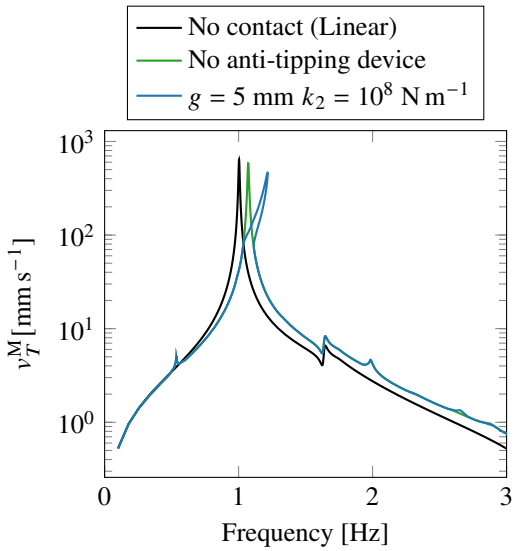

(d) Transversal velocity v_T^{M} on the reduced frequency bandwidth for different configurations.

Figure 21: Frequency responses. HBM parameters: $n_{\mathrm{h}} = 20$, $n_t = 2000$, $\Delta s_{\max} = 0.25$.

5.2.4 Optimization results

The constrained optimization problem (Eq. (42)) is investigated using the presented strategy. Fig. 22 represents several steps of the enrichment process for 20 initial samples. The level curves represent the predictive evolution of the y objective function given by the surrogate model. The red line depicts the limit of the predicted constraint function $\mathrm{h}(g, k_2) = 0$ that delimits the feasible domain . The predictions on both functions are refined along the enrichment process. Fig. 22 shows that the method is able to find a not straightforward global minimum while respecting the constraint with a limited number of HBM solver calls. To better assess the robustness of the method, the optimization is replicated for different initial sampling and for different numbers of initial samples. Fig. 23 depicts the mean and standard deviation of the best value obtained during the process with regard to the number of calls to the mechanical solver. This proves that the proposed strategy efficiently provides the global minimum with a very limited number of evaluations of the expensive objective function. These results are also in line with the conclusion of [49] that a few initial samples should be preferred.

The best obtained parameters for the design of the anti-tipping device are $g^* = 21.47\,\mathrm{mm}$ and $k_2^* = 7.1281 \times$

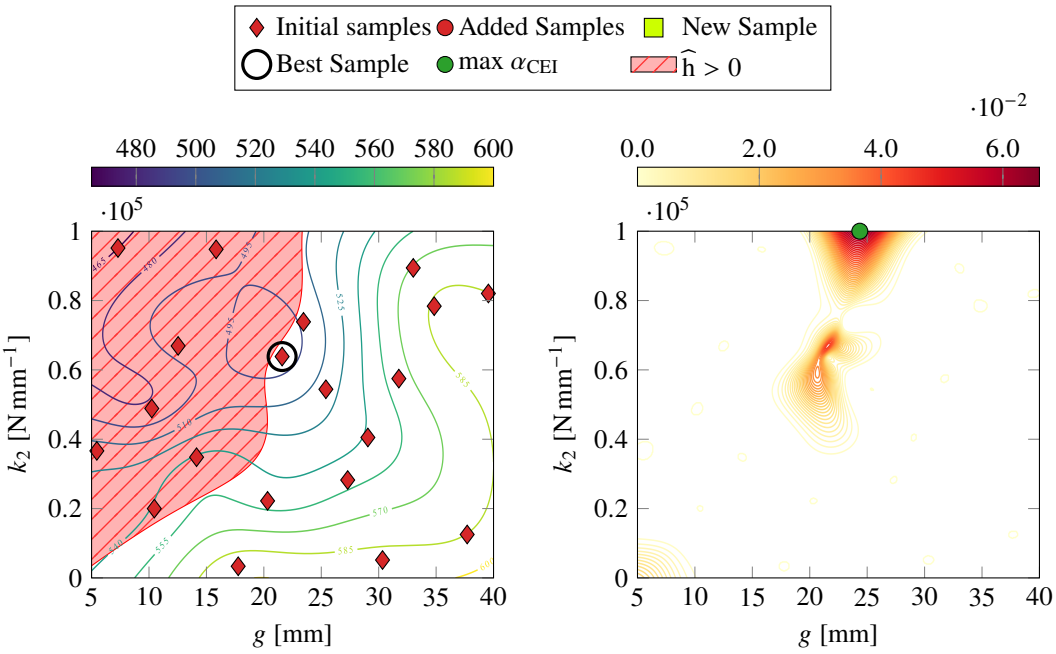

(a1) Predictions $\widehat{\text{y}}$ and $\widehat{\text{h}}$.

(a2) Acquisition Function α_{CEI}.

(a) Initialization.

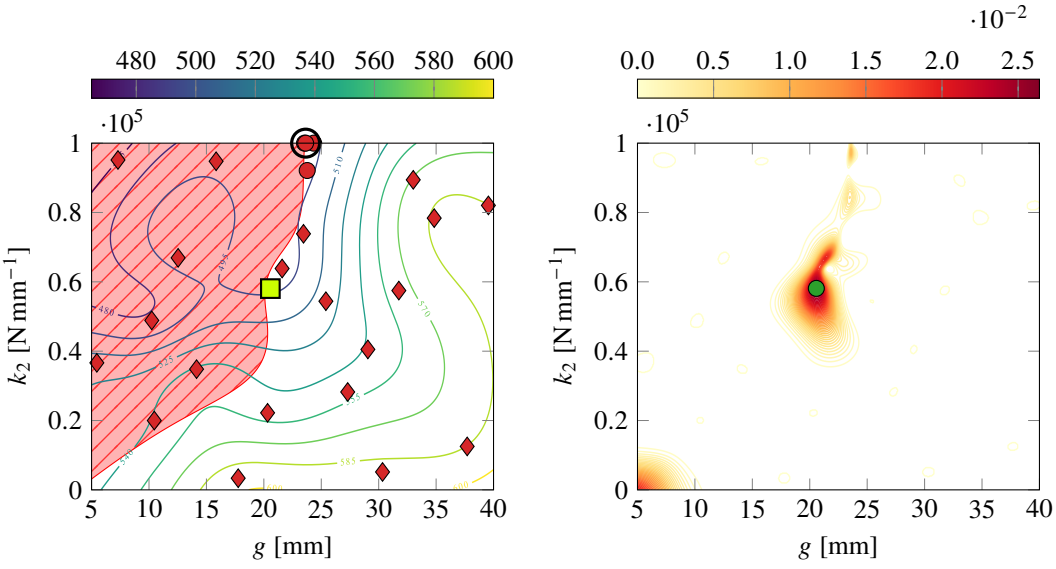

(b1) Predictions $\widehat{\text{y}}$ and $\widehat{\text{h}}$.

(b2) Acquisition Function α_{CEI}.

(b) Iteration 5.

Figure 22: Constrained optimization process for 20 initial samples. Contour lines represent the objective function (in mm s^{-1}), the red hatched area is the predicted unfeasible domain ($\text{h} > 0$) and the black circle indicates the best feasible sampled parameters set.

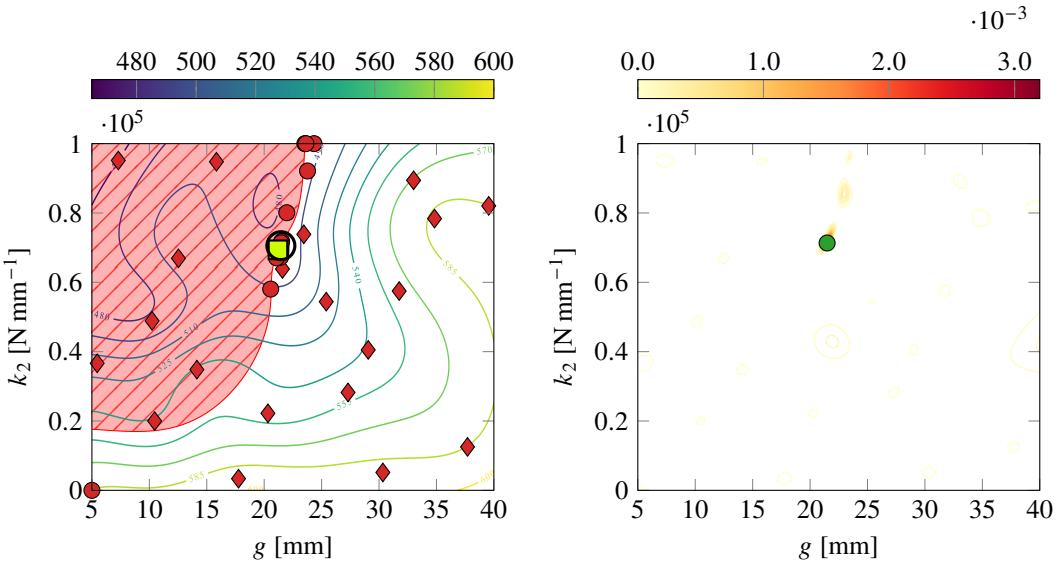

(c1) Predictions $\widehat{y}$ and $\widehat{h}$.

(c2) Acquisition Function α_{CEI}.

(c) Iteration 15.

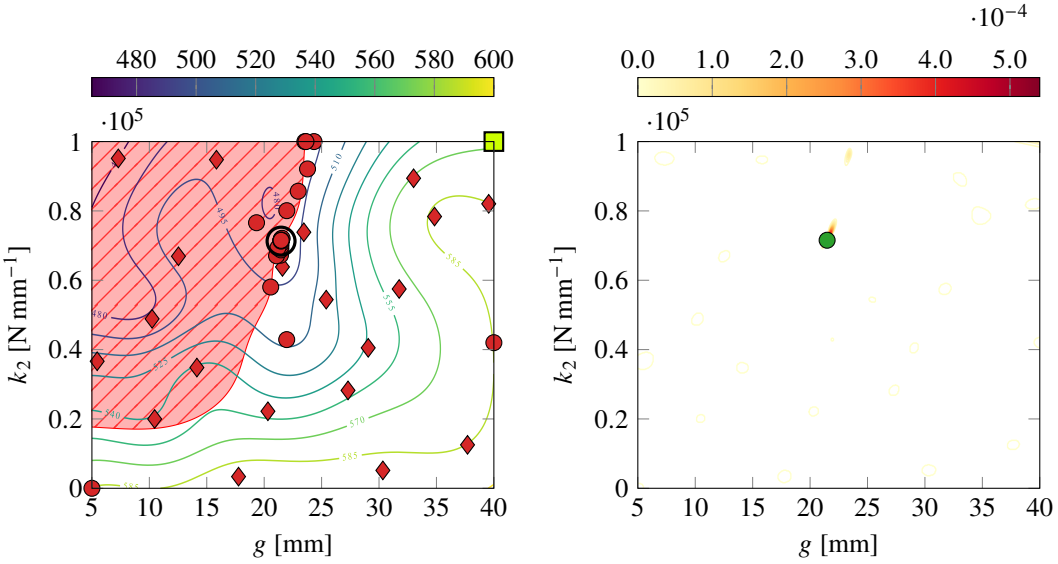

(d1) Predictions $\widehat{y}$ and $\widehat{h}$.

(d2) Acquisition Function α_{CEI}.

(d) Iteration 30.

Figure 22: Constrained optimization process for 20 initial samples (cont.).

$10^7\,\mathrm{N\,m^{-1}}$ which leads to a maximum transversal speed of $484.34\,\mathrm{mm\,s^{-1}}$ and a maximum contact force of 199.992 kN which confirms the optimal parameter set is at the frontier of the feasible domain. The results obtained from the simulation of the gantry crane for the optimal parameters are shown in Fig. 24. Fig. 24a shows that the frequency response behavior of v_T^{M} is similar to Fig. 21 with a fold bifurcation at the frequencies at which the contact with the anti-tipping device may occur. The time representation at the 1.11 Hz peak in Fig. 24c seems sinusoidal, but higher order harmonics are present even if not visible. Fig. 24b confirms that the contact with the anti-tipping device only occurs on a small range of frequencies and its time representation at the peak (Fig. 24d) clearly shows the sporadic contact alternating between the anti-tipping device and the ground. Fig. 24d also

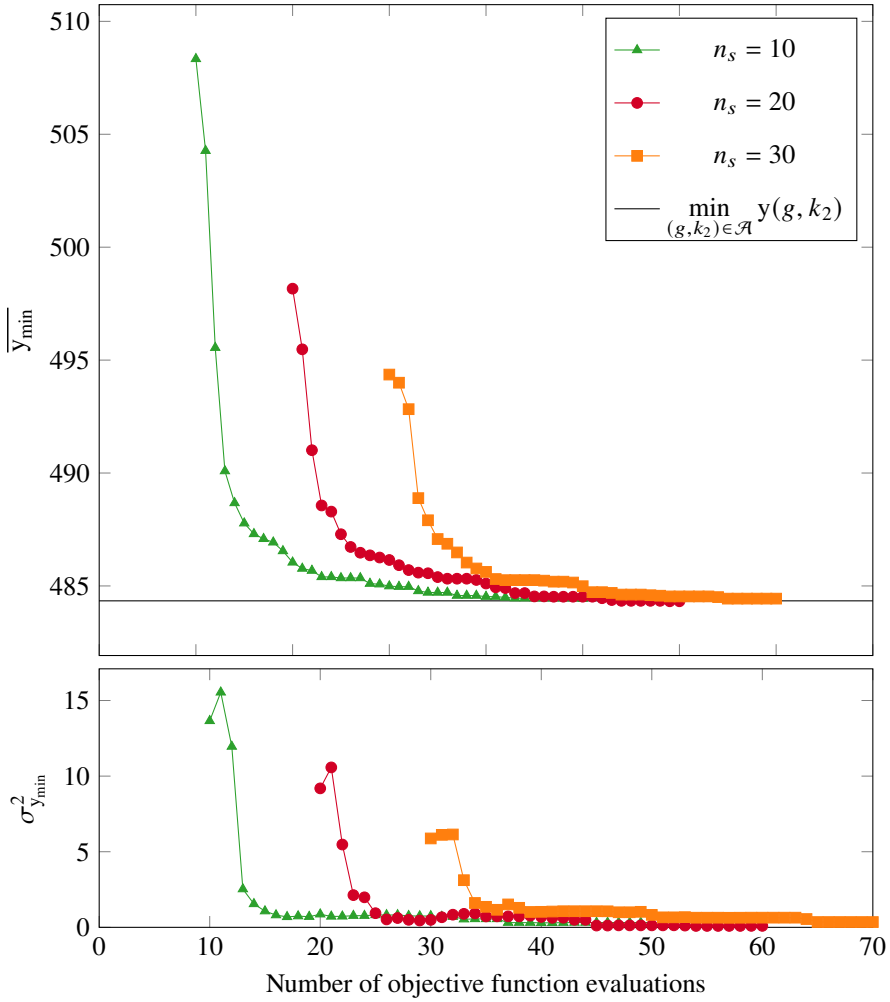

Figure 23: Mean and standard deviation of the best value sampled (in mm s^{-1}) for 10, 20 and 30 initial samples.

showcases the Gibbs phenomenon inherent to the Fourier series.

The *CBO-HBM* strategy is able to solve a constrained optimization problem on a nonlinear industrial structure in vibration. The optimal design parameters of the gantry crane can be accurately obtained with few calls to the mechanical solver, which results in a reasonable computation time. For this specific example, a very small number of initial samples gives the best performances. However, deriving a universal practice from it would not be advisable, as this quantity appears highly dependent on the specific problem at hand. Particularly, the topologies of the objective and constraint functions are important factors, as the example in Section 4.3 shows. Using a budget to define the duration of the enrichment process is straightforward and ensures the computational feasibility of the process. Exploring the implementation of a stopping criterion based on the acquisition function value may nevertheless lead to better performances.

6 Conclusion and discussion

This work aims at proposing an efficient strategy to perform constrained optimization of mechanical structures involving local nonlinearities. The developed *CBO-HBM* workflow is based on the Constrained Bayesian Optimization framework as well as the Harmonic Balance Method to solve mechanical problem. The objective and potential constraint functions are approximated using independent Gaussian Process surrogate models, it-

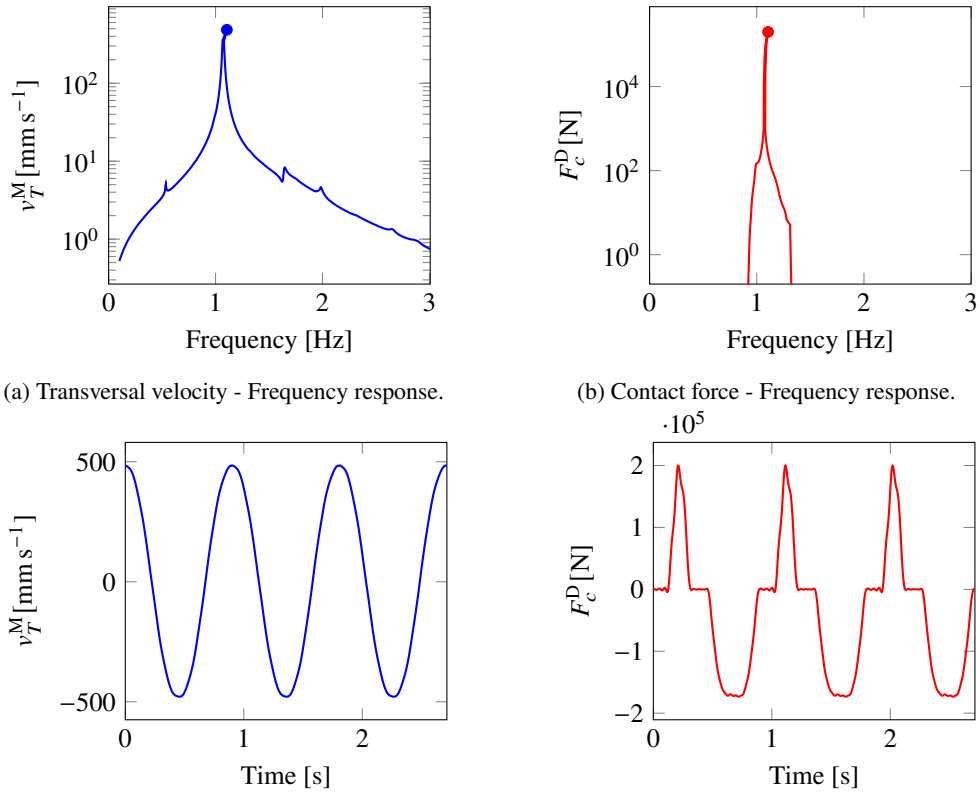

(a) Transversal velocity - Frequency response.

(b) Contact force - Frequency response.

(c) Transversal velocity - Time response.

(d) Contact force - Time response.

Figure 24: Frequency response of v_T^{M} and F_c^{D} as well as their time representations over 3 periods at their maximal value (excitation frequency of 1.11 Hz).

eratively enriched by employing the Constrained Expected Improvement acquisition function. A finite element computation of the structures' frequency responses using the Harmonic Balance Method with a path-following continuation procedure provides the values of the objective and constraint functions for a given set of design parameters while taking into account the nonlinear dynamical effects. Moreover, bifurcations phenomena, which arose commonly in nonlinear vibrations along the frequency range, are depicted which is not possible unlike a classical time-integration solver. Applications on a Duffing oscillator and an industrial-scale gantry crane show the robustness and efficiency of the mechanical solver for a wide range of parameters. The employed Gaussian Processes are able to robustly approximate the nonlinear objective and constraint functions which enables performing a constrained Bayesian Optimization with the CEI acquisition function. Results show that the strategy is able to localize a global minimum fulfilling the constraints with a limited number of expensive mechanical solver calls. The repetition of the strategy with different initial samplings shows consistent results as well as the robustness of the whole method. To further improve the *CBO-HBM* strategy, the mechanical solver may be made more efficient by including the latest developments on the HBM, which is an active field of research. The path-following continuation method plays a huge role in the efficiency of the resolution. Other methods could be investigated as well as a better rule for the length step adaptation in the procedure. For the applications presented in this work, and for many optimization problems in vibrations, only a maximum value of a quantity of interest over a frequency range is used. Therefore, methods able to directly find the resonance peak [67] or to follow the peaks along the parameters [158] present a great interest. However, the choice has been made to compute the whole frequency response with bifurcations to allow the possibility to build objective or constraint functions exploiting the complete dynamical behavior of the structure. Moreover, the constraint and objective functions do not necessarily have their maximal values at the same frequency. Developing a method able to follow the peaks of all the functions at once would be a worth investigating direction of research based for instance on [159].

Conflict of interest

On behalf of all authors, the corresponding author states that there is no conflict of interest.

Replication of results

The developments made are thought to be detailed enough in the present paper to reproduce the strategy. The Python code for the HBM resolution and Bayesian Optimization on the Duffing oscillator can be found on Zenodo archive [160]. As explained in Section 4, the Gaussian Processes are built with the *BoTorch* Python library [98] using a *SingleTaskGP* with a linear mean function and the Matérn kernel. The exact marginal log-likelihood is maximized to fit the hyperparameters. The Bayesian Optimization is performed with the Constrained Expected Improvement acquisition function implemented in *BoTorch*.

Acknowledgements

This work was achieved in the context of a Cifre PhD granted by ANRT (French National Research and Technology Association) - Cifre N° 2020/0272.

References

[1] M. Teichgräber et al. "Non-Linear Structural Models and the Partial Safety Factor Concept." In: *Structural Safety* 103 (July 2023), p. 102341. DOI: 10.1016/j.strusafe.2023.102341 (cit. on p. 2).

[2] K. Kusakana. "Optimal Energy Management of a Retrofitted Rubber Tyred Gantry Crane with Energy Recovery Capabilities." In: *Journal of Energy Storage* 42 (Oct. 2021), p. 103050. DOI: 10.1016/j.est.2021.103050 (cit. on p. 2).

[3] K. Furuta and T. Kanno. "How the Fukushima Daiichi Accident Changed or Not the Nuclear Safety Fundamentals?" In: *Resilience: A New Paradigm of Nuclear Safety: From Accident Mitigation to Resilient Society Facing Extreme Situations*. Ed. by J. Ahn, F. Guarnieri, and K. Furuta. Cham: Springer International Publishing, 2017, pp. 35–45. DOI: 10.1007/978-3-319-58768-4_3 (cit. on p. 2).

[4] J. E. Munoz Garcia, C. Pétesch, and T. Lebarbé. "Adaptation of Standards to Innovative Reactors." In: *ASME 2022 Pressure Vessels & Piping Conference*. Vol. Volume 1: Codes and Standards. Las Vegas, Nevada, USA: American Society of Mechanical Engineers Digital Collection, Nov. 2022. DOI: 10.1115/PVP2022-85479 (cit. on p. 2).

[5] C. G. Corlu et al. "Optimizing Energy Consumption in Transportation: Literature Review, Insights, and Research Opportunities." In: *Energies* 13.5 (Jan. 2020), p. 1115. DOI: 10.3390/en13051115 (cit. on p. 2).

[6] R. R. Craig Jr and M. Bampton. "Coupling of substructures for dynamic analyses." In: *AIAA Journal* 6.7 (1968), pp. 1313–1319. DOI: 10.2514/3.4741 (cit. on pp. 2, 27).

[7] N. Krylov and N. Bogoliuboff. *Introduction to Non-Linear Mechanics*. Vol. 11. Annals of Mathematics Studies. Princeton, NJ, USA: Princeton University Press, 1950. DOI: 10.1515/9781400882274 (cit. on pp. 2–3, 5).

[8] D. R. Jones, M. Schonlau, and W. J. Welch. "Efficient Global Optimization of Expensive Black-Box Functions." In: *Journal of Global Optimization* 13.4 (Dec. 1998), pp. 455–492. DOI: 10.1023/A:1008306431147 (cit. on pp. 2, 4, 9–10, 12, 18).

[9] N. M. Newmark. "A Method of Computation for Structural Dynamics." In: *Journal of the Engineering Mechanics Division* 85.3 (July 1959), pp. 67–94. DOI: 10.1061/JMCEA3.0000098 (cit. on p. 3).

[10] M. A. Dokainish and K. Subbaraj. "A survey of direct time-integration methods in computational structural dynamics—I. Explicit methods." In: *Computers & Structures* 32.6 (Jan. 1989), pp. 1371–1386. DOI: 10.1016/0045-7949(89)90314-3 (cit. on p. 3).

[11] K. Subbaraj and M. A. Dokainish. "A survey of direct time-integration methods in computational structural dynamics—II. Implicit methods." In: *Computers & Structures* 32.6 (Jan. 1989), pp. 1387–1401. DOI: 10.1016/0045-7949(89)90315-5 (cit. on p. 3).

[12] M. Peeters et al. "Nonlinear normal modes, Part II: Toward a practical computation using numerical continuation techniques." In: *Mechanical Systems and Signal Processing*. Special Issue: Non-linear Structural Dynamics 23.1 (Jan. 2009), pp. 195–216. DOI: 10.1016/j.ymssp.2008.04.003 (cit. on p. 3).

[13] P. Sundararajan and S. T. Noah. "Dynamics of Forced Nonlinear Systems Using Shooting/Arc-Length Continuation Method—Application to Rotor Systems." In: *Journal of Vibration and Acoustics* 119.1 (Jan. 1997), pp. 9–20. DOI: 10.1115/1.2889694 (cit. on p. 3).

[14] S. Stoykov and S. Margenov. "Numerical computation of periodic responses of nonlinear large-scale systems by shooting method." In: *Computers & Mathematics with Applications*. Efficient Algorithms for Large Scale Scientific Computations 67.12 (July 2014), pp. 2257–2267. DOI: 10.1016/j.camwa.2014.01.023 (cit. on p. 3).

[15] S. Karkar, B. Cochelin, and C. Vergez. "A comparative study of the harmonic balance method and the orthogonal collocation method on stiff nonlinear systems." In: *Journal of Sound and Vibration* 333.12 (June 2014), pp. 2554–2567. DOI: 10.1016/j.jsv.2014.01.019 (cit. on p. 3).

[16] A. Dhooge et al. "New features of the software MatCont for bifurcation analysis of dynamical systems." In: *Mathematical and Computer Modelling of Dynamical Systems* 14.2 (Apr. 2008), pp. 147–175. DOI: 10.1080/13873950701742754 (cit. on p. 3).

[17] U. Ascher, J. Christiansen, and R. D. Russell. "A collocation solver for mixed order systems of boundary value problems." In: *Mathematics of Computation* 33.146 (1979), pp. 659–679. DOI: 10.1090/S0025-5718-1979-0521281-7 (cit. on p. 3).

[18] E. J. Doedel and B. E. Oldeman. *AUTO-07P: Continuation and bifurcation software for ordinary differential equations*. Montreal, Canada, 2007 (cit. on p. 3).

[19] H. Dankowicz and F. Schilder. *Continuation Core and Toolboxes (COCO)*. 2020 (cit. on p. 3).

[20] H. Dankowicz and F. Schilder. *Recipes for Continuation*. Philadelphia, PA, USA: Society for Industrial and Applied Mathematics, Aug. 2013. DOI: 10.1137/1.9781611972573 (cit. on p. 3).

[21] A. N. Jean and H. D. Nelson. "Periodic response investigation of large order non-linear rotordynamic systems using collocation." In: *Journal of Sound and Vibration* 143.3 (Dec. 1990), pp. 473–489. DOI: 10.1016/0022-460X(90)90737-K (cit. on p. 3).

[22] L. Salles et al. "Dual Time Stepping Algorithms With the High Order Harmonic Balance Method for Contact Interfaces With Fretting-Wear." In: *Journal of Engineering for Gas Turbines and Power* 134.3 (Dec. 2011). DOI: 10.1115/1.4004236 (cit. on p. 3).

[23] M. Nakhla and J. Vlach. "A piecewise harmonic balance technique for determination of periodic response of nonlinear systems." In: *IEEE Transactions on Circuits and Systems* 23.2 (Feb. 1976), pp. 85–91. DOI: 10.1109/TCS.1976.1084181 (cit. on pp. 3, 5).

[24] A. H. Nayfeh and D. T. Mook. *Nonlinear Oscillations*. New York: Wiley, 1979. DOI: 10.1002/9783527617586 (cit. on pp. 3, 5).

[25] S. L. Lau and Y. K. Cheung. "Amplitude Incremental Variational Principle for Nonlinear Vibration of Elastic Systems." In: *Journal of Applied Mechanics* 48.4 (Dec. 1981), pp. 959–964. DOI: 10.1115/1.3157762 (cit. on pp. 3, 5).

[26] Y. K. Cheung and S. L. Lau. "Incremental time—space finite strip method for non-linear structural vibrations." In: *Earthquake Engineering & Structural Dynamics* 10.2 (1982), pp. 239–253. DOI: 10.1002/eqe.4290100206 (cit. on pp. 3, 5).

[27] C. Pierre, A. A. Ferri, and E. H. Dowell. "Multi-Harmonic Analysis of Dry Friction Damped Systems Using an Incremental Harmonic Balance Method." In: *Journal of Applied Mechanics* 52.4 (Dec. 1985), pp. 958–964. DOI: 10.1115/1.3169175 (cit. on pp. 3, 5).

[28] Y. K. Cheung, S. H. Chen, and S. L. Lau. "Application of the incremental harmonic balance method to cubic non-linearity systems." In: *Journal of Sound and Vibration* 140.2 (July 1990), pp. 273–286. DOI: 10.1016/0022-460X(90)90528-8 (cit. on pp. 3, 5).

[29] T. M. Cameron and J. H. Griffin. "An Alternating Frequency/Time Domain Method for Calculating the Steady-State Response of Nonlinear Dynamic Systems." In: *Journal of Applied Mechanics* 56.1 (Mar. 1989), pp. 149–154. DOI: 10.1115/1.3176036 (cit. on pp. 3, 6).

[30] E. Sarrouy and J.-J. Sinou. "Non-Linear Periodic and Quasi-Periodic Vibrations in Mechanical Systems - On the use of the Harmonic Balance Methods." In: *Advances in Vibration Analysis Research*. Ed. by F. Ebrahimi. Rijeka: IntechOpen, Apr. 2011. Chap. 21, pp. 419–434. DOI: 10.5772/15638 (cit. on pp. 3, 9).

[31] O. Poudou and C. Pierre. "Hybrid Frequency-Time Domain Methods for the Analysis of Complex Structural Systems with Dry Friction Damping." In: *44th AIAA/ASME/ASCE/AHS/ASC Structures, Structural Dynamics, and Materials Conference*. Norfolk, Virginia: American Institute of Aeronautics and Astronautics, 2003. DOI: 10.2514/6.2003-1411 (cit. on p. 3).

[32] A. Mabilia et al. "Nonlinear Forced Response of a Composite Fan Blade Actuated by Piezoelectric Patches: Simulation and Testing." In: *Nonlinear Dynamics, Volume 1*. Ed. by G. Kerschen. Conference Proceedings of the Society for Experimental Mechanics Series. Cham: Springer International Publishing, 2019, pp. 351–362. DOI: 10.1007/978-3-319-74280-9_37 (cit. on p. 3).

[33] T. Vadcard et al. "Assessment of Two Harmonic Balance Method-Based Numerical Strategies for Blade-Tip/Casing Interactions: Application to NASA Rotor 67." In: *Journal of Engineering for Gas Turbines and Power* 144.12 (Oct. 2022), p. 121004. DOI: 10.1115/1.4055416 (cit. on p. 3).

[34] E. H. Moussi. "Analyse de structures vibrantes dotées de non-linéarités localisées à jeu à l'aide des modes non-linéaires." PhD Thesis. France: Université d'Aix-Marseille, Dec. 2013 (cit. on p. 3).

[35] R. Alcorta Galvan. "Prediction of non-linear responses and bifurcations of impacting systems : Contribution to the understanding of steam generator vibrations." PhD Thesis. France: INSA de Lyon, May 2021 (cit. on p. 3).

[36] T. Detroux et al. "The harmonic balance method for bifurcation analysis of large-scale nonlinear mechanical systems." In: *Computer Methods in Applied Mechanics and Engineering* 296 (Nov. 2015), pp. 18–38. DOI: 10.1016/j.cma.2015.07.017 (cit. on p. 3).

[37] V. Jaumouillé, J.-J. Sinou, and B. Petitjean. "Simulation of Payne Effect of Elastomeric Isolators with a Harmonic Balance Method." In: *Shock and Vibration* 19 (2012), pp. 1281–1295. DOI: 10.3233/SAV-2012-0670 (cit. on p. 3).

[38] M. Krack and J. Gross. *Harmonic Balance for Nonlinear Vibration Problems*. Mathematical Engineering. Cham: Springer International Publishing, 2019. DOI: 10.1007/978-3-030-14023-6 (cit. on pp. 3, 8–9).

[39] P. W. Christensen and A. Klarbring. *An Introduction to Structural Optimization*. Vol. 153. Solid Mechanics and Its Applications. Dordrecht: Springer Netherlands, 2008. DOI: 10.1007/978-1-4020-8666-3 (cit. on p. 3).

[40] A. L. Cauchy. "Méthode générale pour la résolution des systemes d'équations simultanées." In: *Comptes Rendus de l'Academie des Science* 25 (1847), pp. 536–538 (cit. on pp. 3, 19).

[41] J. Nocedal and S. J. Wright. "Quasi-Newton Methods." In: *Numerical Optimization*. Springer Series in Operations Research and Financial Engineering. New York, NY: Springer New York, 2006, pp. 135–163. DOI: 10.1007/978-0-387-40065-5_6 (cit. on p. 3).

[42] S. Kirkpatrick, C. D. Gelatt, and M. P. Vecchi. "Optimization by Simulated Annealing." In: *Science* 220.4598 (May 1983), pp. 671–680. DOI: 10.1126/science.220.4598.671 (cit. on pp. 3, 9).

[43] T. Back, U. Hammel, and H.-P. Schwefel. "Evolutionary computation: comments on the history and current state." In: *IEEE Transactions on Evolutionary Computation* 1.1 (Apr. 1997), pp. 3–17. DOI: 10.1109/4235.585888 (cit. on pp. 3, 9).

[44] M. Dorigo, M. Birattari, and T. Stutzle. "Ant colony optimization." In: *IEEE Computational Intelligence Magazine* 1.4 (Nov. 2006), pp. 28–39. DOI: 10.1109/MCI.2006.329691 (cit. on pp. 4, 9).

[45] J. Kennedy and R. Eberhart. "Particle swarm optimization." In: *Proceedings of ICNN'95 - International Conference on Neural Networks*. Vol. 4. Perth, WA, Australia, Nov. 1995, pp. 1942–1948. DOI: 10.1109/ICNN.1995.488968 (cit. on pp. 4, 9).

[46] N. V. Queipo et al. "Surrogate-based analysis and optimization." In: *Progress in Aerospace Sciences* 41.1 (Jan. 2005), pp. 1–28. DOI: 10.1016/j.paerosci.2005.02.001 (cit. on p. 4).

[47] J. Mockus, V. Tiesis, and A. Zilinskas. "The application of Bayesian methods for seeking the extremum." In: *Towards Global Optimization*. Ed. by L. Dixon and G. Szegö. Vol. 2. Amsterdam: North-Holland, 1978, pp. 117–129 (cit. on pp. 4, 9).

[48] P. I. Frazier. *A Tutorial on Bayesian Optimization*. July 2018. DOI: 10.48550/ARXIV.1807.02811 (cit. on p. 4).

[49] R. Le Riche and V. Picheny. "Revisiting Bayesian optimization in the light of the COCO benchmark." In: *Structural and Multidisciplinary Optimization* 64.5 (Nov. 2021), pp. 3063–3087. DOI: 10.1007/s00158-021-02977-1 (cit. on pp. 4, 10, 15, 20, 28).

[50] C. E. Rasmussen and C. K. I. Williams. *Gaussian Processes for Machine Learning*. Cambridge, Massachusetts: The MIT Press, Nov. 2006. DOI: 10.7551/mitpress/3206.001.0001 (cit. on pp. 4, 10).

[51] R. B. Gramacy. *Surrogates: Gaussian Process Modeling, Design and Optimization for the Applied Sciences*. Boca Raton, Florida: Chapman Hall/CRC, 2020. DOI: 10.1201/9780367815493 (cit. on pp. 4, 9).

[52] Y. Shen et al. "Parameters optimization for a novel dynamic vibration absorber." In: *Mechanical Systems and Signal Processing* 133 (Nov. 2019), p. 106282. DOI: 10.1016/j.ymssp.2019.106282 (cit. on p. 4).

[53] A. Y. T. Leung and H. Zhang. "Particle swarm optimization of tuned mass dampers." In: *Engineering Structures* 31.3 (Mar. 2009), pp. 715–728. DOI: 10.1016/j.engstruct.2008.11.017 (cit. on p. 4).

[54] F. A. C. Viana et al. "Tuning dynamic vibration absorbers by using ant colony optimization." In: *Computers & Structures* 86.13 (July 2008), pp. 1539–1549. DOI: 10.1016/j.compstruc.2007.05.009 (cit. on p. 4).

[55] A. Klarbring. "On the Problem of Optimizing Contact Force Distributions." In: *Journal of Optimization Theory and Applications* 74.1 (July 1992), pp. 131–150. DOI: 10.1007/BF00939896 (cit. on p. 4).

[56] P. Beremlijski et al. "Shape Optimization in Contact Problems with Coulomb Friction." In: *SIAM Journal on Optimization* 13.2 (2002), pp. 561–587. DOI: 10.1137/S1052623401395061 (cit. on p. 4).

[57] A. Myśliński and M. Wróblewski. "Structural Optimization of Contact Problems Using Cahn–Hilliard Model." In: *Computers & Structures* 180 (2017), pp. 52–59. DOI: 10.1016/j.compstruc.2016.03.013 (cit. on p. 4).

[58] W. Zhang and C. Niu. "A Linear Relaxation Model for Shape Optimization of Constrained Contact Force Problem." In: *Computers & Structures* 200 (2018), pp. 53–67. DOI: 10.1016/j.compstruc.2018.02.005 (cit. on p. 4).

[59] Z. .-. Ma, N. Kikuchi, and I. Hagiwara. "Structural Topology and Shape Optimization for a Frequency Response Problem." In: *Computational Mechanics* 13.3 (Dec. 1993), pp. 157–174. DOI: 10.1007/BF00370133 (cit. on p. 4).

[60] H.-A. Lee and G.-J. Park. "Nonlinear Dynamic Response Topology Optimization Using the Equivalent Static Loads Method." In: *Computer Methods in Applied Mechanics and Engineering* 283 (Jan. 2015), pp. 956–970. DOI: 10.1016/j.cma.2014.10.015 (cit. on p. 4).

[61] R. Behrou and J. K. Guest. "Topology Optimization for Transient Response of Structures Subjected to Dynamic Loads." In: *18th AIAA/ISSMO Multidisciplinary Analysis and Optimization Conference*. AIAA AVIATION Forum. Denver, Colorado, USA: American Institute of Aeronautics and Astronautics, June 2017. DOI: 10.2514/6.2017-3657 (cit. on p. 4).

[62] V. Shobeiri. "Bidirectional Evolutionary Structural Optimization for Nonlinear Structures under Dynamic Loads." In: *International Journal for Numerical Methods in Engineering* 121.5 (2020), pp. 888–903. DOI: 10.1002/nme.6249 (cit. on p. 4).

[63] E. Raponi et al. "Kriging-Assisted Topology Optimization of Crash Structures." In: *Computer Methods in Applied Mechanics and Engineering* 348 (May 2019), pp. 730–752. DOI: 10.1016/j.cma.2019.02.002 (cit. on p. 4).

[64] E. Raponi et al. "Hybrid Strategy Coupling EGO and CMA-ES for Structural Topology Optimization in Statics and Crashworthiness." In: *Computational Intelligence*. Ed. by J. J. Merelo et al. Studies in Computational Intelligence. Cham: Springer International Publishing, 2021, pp. 55–84. DOI: 10.1007/978-3-030-70594-7_3 (cit. on p. 4).

[65] E. Denimal et al. "Topological Optimization of Under-Platform Dampers With Moving Morphable Components and Global Optimization Algorithm for Nonlinear Frequency Response." In: *Journal of Engineering for Gas Turbines and Power* 143.021021 (Feb. 2021). DOI: 10.1115/1.4049666 (cit. on p. 4).

[66] Q. Lin et al. "Design of Component Structure in Assemblies for Simultaneously Regulating Contact Pressure Distribution and Natural Frequencies." In: *European Journal of Mechanics - A/Solids* 94 (2022), p. 104557. DOI: 10.1016/j.euromechsol.2022.104557 (cit. on p. 4).

[67] E. Denimal et al. "Topology optimisation of friction under-platform dampers using moving morphable components and the efficient global optimization algorithm." In: *Structural and Multidisciplinary Optimization* 65.2 (Jan. 2022), p. 56. DOI: 10.1007/s00158-021-03158-w (cit. on pp. 4, 32).

[68] K. Liu, D. Detwiler, and A. Tovar. "Optimal Design of Nonlinear Multimaterial Structures for Crashworthiness Using Cluster Analysis." In: *Journal of Mechanical Design* 139.101401 (Aug. 2017). DOI: 10.1115/1.4037620 (cit. on p. 4).

[69] C. Ren, H.-t. Min, and T.-f. Ma. "An Efficient Topology Optimization Strategy for Structural Crashworthiness Using Model and ESLs Reduction Method." In: *DEStech Transactions on Computer Science and Engineering* (2019). DOI: 10.12783/dtcse/iteee2019/28769 (cit. on p. 4).

[70] P. Zakian and A. Kaveh. "Multi-Objective Seismic Design Optimization of Structures: A Review." In: *Archives of Computational Methods in Engineering* (Sept. 2023). DOI: 10.1007/s11831-023-09992-z (cit. on p. 4).

[71] Y.-I. Kim and G.-J. Park. "Nonlinear dynamic response structural optimization using equivalent static loads." In: *Computer Methods in Applied Mechanics and Engineering* 199.9 (2010), pp. 660–676. DOI: https://doi.org/10.1016/j.cma.2009.10.014 (cit. on p. 4).

[72] G.-J. Park. "Technical overview of the equivalent static loads method for non-linear static response structural optimization." In: *Structural and Multidisciplinary Optimization* 43.3 (2011), pp. 319–337. DOI: 10.1007/s00158-010-0530-x (cit. on p. 4).

[73] H. H. Jang et al. "Dynamic Response Topology Optimization in the Time Domain Using Equivalent Static Loads." In: *AIAA Journal* 50.1 (Jan. 2012), pp. 226–234. DOI: 10.2514/1.J051256 (cit. on p. 4).

[74] M. Al-Bazoon and J. S. Arora. "Discrete variable optimization of structures subjected to dynamic loads using equivalent static loads and metaheuristic algorithms." In: *Optimization and Engineering* 23.2 (2022), pp. 643–687. DOI: 10.1007/s11081-021-09599-y (cit. on p. 4).

[75] M. Al-Bazoon and J. S. Arora. "Optimization of framed structures subjected to blast loading using equivalent static loads method." In: *Asian Journal of Civil Engineering* 24.8 (Dec. 2023), pp. 3305–3318. DOI: 10.1007/s42107-023-00711-4 (cit. on p. 4).

[76] B.-S. Kang, G.-J. Park, and J. S. Arora. "A review of optimization of structures subjected to transient loads." In: *Structural and Multidisciplinary Optimization* 31.2 (2006), pp. 81–95. DOI: 10.1007/s00158-005-0575-4 (cit. on p. 4).

[77] S. Dou and J. S. Jensen. "Optimization of nonlinear structural resonance using the incremental harmonic balance method." In: *Journal of Sound and Vibration* 334 (Jan. 2015), pp. 239–254. DOI: 10.1016/j.jsv.2014.08.023 (cit. on p. 4).

[78] S. Dou et al. "Structural Optimization for Nonlinear Dynamic Response." In: *Philosophical Transactions of the Royal Society A: Mathematical, Physical and Engineering Sciences* 373.2051 (Sept. 2015), p. 20140408. DOI: 10.1098/rsta.2014.0408 (cit. on p. 4).

[79] Y. Yuan et al. "Robust design optimisation of underplatform dampers for turbine applications using a surrogate model." In: *Journal of Sound and Vibration* 494 (Mar. 2021), p. 115528. DOI: 10.1016/j.jsv.2020.115528 (cit. on p. 4).

[80] M. Krack et al. "Reliability optimization of friction-damped systems using nonlinear modes." In: *Journal of Sound and Vibration* 333.13 (June 2014), pp. 2699–2712. DOI: 10.1016/j.jsv.2014.02.008 (cit. on p. 4).

[81] T. Detroux, J.-P. Noël, and G. Kerschen. "Tailoring the Resonances of Nonlinear Mechanical Systems." In: *Nonlinear Dynamics* 103.4 (Mar. 2021), pp. 3611–3624. DOI: 10.1007/s11071-020-06002-w (cit. on p. 4).

[82] E. Boroson and S. Missoum. "Stochastic optimization of nonlinear energy sinks." In: *Structural and Multidisciplinary Optimization* 55.2 (Feb. 2017), pp. 633–646. DOI: 10.1007/s00158-016-1526-y (cit. on p. 4).

[83] M. Urabe. "Galerkin's procedure for nonlinear periodic systems." In: *Archive for Rational Mechanics and Analysis* 20.2 (Jan. 1965), pp. 120–152. DOI: 10.1007/BF00284614 (cit. on p. 6).

[84] P. Deuflhard. *Newton Methods for Nonlinear Problems*. Vol. 35. Springer Series in Computational Mathematics. Berlin, Heidelberg: Springer Verlag, 2011. DOI: 10.1007/978-3-642-23899-4 (cit. on p. 6).

[85] C. Shannon. "Communication in the Presence of Noise." In: *Proceedings of the IRE* 37.1 (Jan. 1949), pp. 10–21. DOI: 10.1109/JRPROC.1949.232969 (cit. on p. 7).

[86] L. Woiwode et al. "Comparison of two algorithms for Harmonic Balance and path continuation." In: *Mechanical Systems and Signal Processing* 136 (Feb. 2020), p. 106503. DOI: 10.1016/j.ymssp.2019.106503 (cit. on pp. 7–8).

[87] J. W. Cooley and J. W. Tukey. "An algorithm for the machine calculation of complex Fourier series." In: *Mathematics of Computation* 19.90 (1965), pp. 297–301. DOI: 10.1090/S0025-5718-1965-0178586-1 (cit. on p. 7).

[88] S. Narayanan and P. Sekar. "A Frequency Domain Based Numeric-Analytical Method for Non-Linear Dynamical Systems." In: *Journal of Sound and Vibration* 211.3 (Apr. 1998), pp. 409–424. DOI: 10.1006/jsvi.1997.1319 (cit. on p. 7).

[89] A. Cardona, A. Lerusse, and M. Géradin. "Fast Fourier nonlinear vibration analysis." In: *Computational Mechanics* 22.2 (Aug. 1998), pp. 128–142. DOI: 10.1007/s004660050347 (cit. on pp. 7–8).

[90] Y. Colaïtis and A. Batailly. "The harmonic balance method with arc-length continuation in blade-tip/casing contact problems." In: *Journal of Sound and Vibration* 502 (June 2021), p. 116070. DOI: 10.1016/j.jsv.2021.116070 (cit. on pp. 7, 9, 24).

[91] G. Von Groll and D. J. Ewins. "The Harmonic Balance Method with Arc-Length Continuation in Rotor/Stator Contact Problems." In: *Journal of Sound and Vibration* 241.2 (Mar. 2001), pp. 223–233. DOI: 10.1006/jsvi.2000.3298 (cit. on p. 8).

[92] E. L. Allgower and K. Georg. *Numerical Continuation Methods*. Vol. 13. Springer Series in Computational Mathematics. Berlin, Heidelberg: Springer-Verlag, 1990. DOI: 10.1007/978-3-642-61257-2 (cit. on pp. 8–9).

[93] R. Seydel. *Practical Bifurcation and Stability Analysis*. Third Edition. Vol. 5. Interdisciplinary Applied Mathematics. New York, NY: Springer-Verlag, 2009 (cit. on p. 8).

[94] B. Cochelin and C. Vergez. "A high order purely frequency-based harmonic balance formulation for continuation of periodic solutions." In: *Journal of Sound and Vibration* 324.1 (July 2009), pp. 243–262. DOI: 10.1016/j.jsv.2009.01.054 (cit. on p. 8).

[95] L. Guillot, B. Cochelin, and C. Vergez. "A generic and efficient Taylor series–based continuation method using a quadratic recast of smooth nonlinear systems." In: *International Journal for Numerical Methods in Engineering* 119.4 (2019), pp. 261–280. DOI: 10.1002/nme.6049 (cit. on p. 8).

[96] H. B. Keller. "The Bordering Algorithm and Path Following Near Singular Points of Higher Nullity." In: *SIAM Journal on Scientific and Statistical Computing* 4.4 (Dec. 1983), pp. 573–582. DOI: 10.1137/0904039 (cit. on p. 8).

[97] W.-J. Beyn et al. "Chapter 4 - Numerical Continuation, and Computation of Normal Forms." In: *Handbook of Dynamical Systems*. Ed. by B. Fiedler. Vol. 2. Handbook of Dynamical Systems. Amsterdam: Elsevier Science, Jan. 2002, pp. 149–219. DOI: 10.1016/S1874-575X(02)80025-X (cit. on p. 9).

[98] M. Balandat et al. "BoTorch: A Framework for Efficient Monte-Carlo Bayesian Optimization." In: *Advances in Neural Information Processing Systems*. Vol. 33. virtual: Curran Associates, Inc., 2020, pp. 21524–21538 (cit. on pp. 9, 33).

[99] J. Gardner et al. "GPyTorch: Blackbox Matrix-Matrix Gaussian Process Inference with GPU Acceleration." In: *Advances in Neural Information Processing Systems*. Vol. 31. Montréal, Canada: Curran Associates, Inc., 2018 (cit. on p. 9).

[100] X. Wang et al. "Recent Advances in Bayesian Optimization." In: *ACM Computing Surveys* 55.13s (July 2023), 287:1–287:36. DOI: 10.1145/3582078 (cit. on p. 9).

[101] C. He et al. "A Review of Surrogate-Assisted Evolutionary Algorithms for Expensive Optimization Problems." In: *Expert Systems with Applications* 217 (May 2023), p. 119495. DOI: 10.1016/j.eswa.2022.119495 (cit. on p. 9).

[102] A. I. J. Forrester, A. Sóbester, and A. J. Keane. *Engineering Design via Surrogate Modelling: A Practical Guide*. Chichester: John Wiley & Sons Ltd, 2008. DOI: 10.1002/9780470770801 (cit. on p. 10).

[103] A. A. Giunta and L. T. Watson. "A comparison of approximation modeling techniques - Polynomial versus interpolating models." In: *AIAA paper 98-4758. 7th AIAA/USAF/NASA/ISSMO Symposium on Multidisciplinary Analysis and Optimization*. St. Louis, MO, USA, Sept. 1998. DOI: 10.2514/6.1998-4758 (cit. on p. 10).

[104] R. Jin, W. Chen, and T. Simpson. "Comparative Studies Of Metamodeling Techniques Under Multiple Modelling Criteria." In: *Structural and Multidisciplinary Optimization* 23 (Dec. 1, 2001), pp. 1–13. DOI: 10.1007/s00158-001-0160-4 (cit. on p. 10).

[105] S. Varadarajan, W. Chen, and C. J. Pelka. "Robust concept exploration of propulsion systems with enhanced model approximation capabilities." In: *Engineering Optimization* 32.3 (2000), pp. 309–334. DOI: doi:10.1080/03052150008941302 (cit. on p. 10).

[106] T. W. Simpson et al. "Metamodels for computer-based engineering design: survey and recommendations." In: *Engineering with Computers* 17.2 (2001), pp. 129–150. DOI: 10.1007/PL00007198 (cit. on p. 10).

[107] B.-S. Kim, Y.-B. Lee, and D.-H. Choi. "Comparison study on the accuracy of metamodeling technique for non-convex functions." In: *Journal of Mechanical Science and Technology* 23.4 (Apr. 2009), pp. 1175–1181. DOI: 10.1007/s12206-008-1201-3 (cit. on p. 10).

[108] D. Zhao and D. Xue. "A comparative study of metamodeling methods considering sample quality merits." English. In: *Structural and Multidisciplinary Optimization* 42.6 (2010), pp. 923–938. DOI: 10.1007/s00158-010-0529-3 (cit. on p. 10).

[109] S. E. Davis, S. Cremaschi, and M. R. Eden. "Efficient Surrogate Model Development: Impact of Sample Size and Underlying Model Dimensions." In: *13th International Symposium on Process Systems Engineering (PSE 2018)*. Ed. by M. R. Eden, M. G. Ierapetritou, and G. P. Towler. Vol. 44. Computer Aided Chemical Engineering. Amsterdam: Elsevier, 2018, pp. 979–984. DOI: 10.1016/B978-0-444-64241-7.50158-0 (cit. on p. 10).

[110] A. Garbo and B. J. German. "Performance Assessment of a Cross-Validation Sampling Strategy with Active Surrogate Model Selection." In: *Structural and Multidisciplinary Optimization* 59.6 (June 2019), pp. 2257–2272. DOI: 10.1007/s00158-018-02190-7 (cit. on p. 10).

[111] J. Prakash and E. J. Joy. "A Comparison of Different Surrogate Models for Delamination Detection in Composite Laminates Using Experimental Modal Analysis." In: *AIP Conference Proceedings* 2270.1 (Nov. 2020), p. 140005. DOI: 10.1063/5.0019366 (cit. on p. 10).

[112] J. Hoole et al. "Comparison of Surrogate Modeling Methods for Finite Element Analysis of Landing Gear Loads." In: *AIAA Scitech 2020 Forum*. Orlando, FL: American Institute of Aeronautics and Astronautics, Jan. 2020. DOI: 10.2514/6.2020-0681 (cit. on p. 10).

[113] S. Funk, A. Airoud Basmaji, and U. Nackenhorst. "Globally Supported Surrogate Model Based on Support Vector Regression for Nonlinear Structural Engineering Applications." In: *Archive of Applied Mechanics* 93.2 (Feb. 2023), pp. 825–839. DOI: 10.1007/s00419-022-02301-3 (cit. on p. 10).

[114] Y. Zhao et al. "Surrogate Modeling of Nonlinear Dynamic Systems: A Comparative Study." In: *Journal of Computing and Information Science in Engineering* 23.1 (Feb. 2023). DOI: 10.1115/1.4054039 (cit. on p. 10).

[115] T. Simpson et al. "Comparison Of Response Surface And Kriging Models For Multidisciplinary Design Optimization." In: *AIAA paper 98-4755. 7th AIAA/USAF/NASA/ISSMO Symposium on Multidisciplinary Analysis and Optimization*. St. Louis, MO, USA, Sept. 1998. DOI: 10.2514/6.1998-4755 (cit. on p. 10).

[116] R. Jin, X. Du, and W. Chen. "The use of metamodeling techniques for optimization under uncertainty." English. In: *Structural and Multidisciplinary Optimization* 25.2 (2003), pp. 99–116. DOI: 10.1007/s00158-002-0277-0 (cit. on p. 10).

[117] N. Stander et al. "A Comparison of Metamodeling Techniques for Crashworthiness Optimization." In: *10th AIAA/ISSMO Multidisciplinary Analysis and Optimization Conference*. Albany, New York: American Institute of Aeronautics and Astronautics, Aug. 2004. DOI: 10.2514/6.2004-4489 (cit. on p. 10).

[118] Y. Jin. "A comprehensive survey of fitness approximation in evolutionary computation." In: *Soft Computing-A Fusion of Foundations, Methodologies and Applications* 9.1 (2005), pp. 3–12. DOI: 10.1007/s00500-003-0328-5 (cit. on p. 10).

[119] H. Fang et al. "A Comparative Study of Metamodeling Methods for Multiobjective Crashworthiness Optimization." In: *Computers & Structures* 83.25 (Sept. 2005), pp. 2121–2136. DOI: 10.1016/j.compstruc.2005.02.025 (cit. on p. 10).

[120] R. R. Barton and M. Meckesheimer. "Chapter 18 Metamodel-Based Simulation Optimization." In: *Handbooks in Operations Research and Management Science*. Ed. by S. G. Henderson and B. L. Nelson. Vol. 13. Simulation. Amsterdam: Elsevier, Jan. 2006, pp. 535–574. DOI: 10.1016/S0927-0507(06)13018-2 (cit. on p. 10).

[121] J. Peter and M. Marcelet. "Comparison of surrogate models for turbomachinery design." In: *WSEAS Transactions on Fluid Dynamics* 3.1 (2008), pp. 10–17 (cit. on p. 10).

[122] R. M. Paiva et al. "Comparison of Surrogate Models in a Multidisciplinary Optimization Framework for Wing Design." In: *AIAA Journal* 48.5 (May 2010), pp. 995–1006. DOI: 10.2514/1.45790 (cit. on p. 10).

[123] B. Eisenhower et al. "A Methodology for Meta-Model Based Optimization in Building Energy Models." In: *Energy and Buildings* 47 (Apr. 2012), pp. 292–301. DOI: 10.1016/j.enbuild.2011.12.001 (cit. on p. 10).

[124] F. A. C. Viana, R. T. Haftka, and L. T. Watson. "Efficient global optimization algorithm assisted by multiple surrogate techniques." In: *Journal of Global Optimization* 56.2 (2013), pp. 669–689. DOI: 10.1007/s10898-012-9892-5 (cit. on p. 10).

[125] L. Leifsson and S. Koziel. "Surrogate Modelling and Optimization Using Shape-Preserving Response Prediction: A Review." In: *Engineering Optimization* 48.3 (Mar. 2016), pp. 476–496. DOI: 10.1080/0305215X.2015.1016509 (cit. on p. 10).

[126] A. Bhosekar and M. Ierapetritou. "Advances in Surrogate Based Modeling, Feasibility Analysis, and Optimization: A Review." In: *Computers & Chemical Engineering* 108 (Jan. 2018), pp. 250–267. DOI: 10.1016/j.compchemeng.2017.09.017 (cit. on p. 10).

[127] R. Yondo et al. "A Review of Surrogate Modeling Techniques for Aerodynamic Analysis and Optimization: Current Limitations and Future Challenges in Industry." In: *Advances in Evolutionary and Deterministic Methods for Design, Optimization and Control in Engineering and Sciences*. Ed. by E. Minisci et al. Computational Methods in Applied Sciences. Cham: Springer International Publishing, 2019, pp. 19–33. DOI: 10.1007/978-3-319-89988-6_2 (cit. on p. 10).

[128] V. Christelis, G. Kopsiaftis, and A. Mantoglou. "Performance Comparison of Multiple and Single Surrogate Models for Pumping Optimization of Coastal Aquifers." In: *Hydrological Sciences Journal* 64.3 (Feb. 2019), pp. 336–349. DOI: 10.1080/02626667.2019.1584400 (cit. on p. 10).

[129] T. Chatterjee, S. Chakraborty, and R. Chowdhury. "A Critical Review of Surrogate Assisted Robust Design Optimization." In: *Archives of Computational Methods in Engineering* 26.1 (Jan. 2019), pp. 245–274. DOI: 10.1007/s11831-017-9240-5 (cit. on p. 10).

[130] T. Nguyen et al. "Comparative Study of Surrogate Modeling Methods for Signal Integrity and Microwave Circuit Applications." In: *IEEE Transactions on Components, Packaging and Manufacturing Technology* 11.9 (Sept. 2021), pp. 1369–1379. DOI: 10.1109/TCPMT.2021.3098666 (cit. on p. 10).

[131] G. Delazeri, M. Ritt, and M. de Souza. "Comparing Surrogate Models for Tuning Optimization Algorithms." In: *Learning and Intelligent Optimization*. Ed. by D. E. Simos et al. Lecture Notes in Computer Science. Cham: Springer International Publishing, 2022, pp. 347–360. DOI: 10.1007/978-3-031-24866-5_26 (cit. on p. 10).

[132] A. Mukhtar, A. S. H. M. Yasir, and M. F. M. Nasir. "A Machine Learning-Based Comparative Analysis of Surrogate Models for Design Optimisation in Computational Fluid Dynamics." In: *Heliyon* 9.8 (Aug. 2023), e18674. DOI: 10.1016/j.heliyon.2023.e18674 (cit. on p. 10).

[133] Y. Ju, C. Zhang, and L. Ma. "Artificial Intelligence Metamodel Comparison and Application to Wind Turbine Airfoil Uncertainty Analysis." In: *Advances in Mechanical Engineering* 8.5 (May 2016), p. 1687814016647317. DOI: 10.1177/1687814016647317 (cit. on p. 10).

[134] C. Wang et al. "Recent Advances in Surrogate Modeling Methods for Uncertainty Quantification and Propagation." In: *Symmetry* 14.6 (2022). DOI: 10.3390/sym14061219 (cit. on p. 10).

[135] M. G. Fernández-Godino. *Review of Multi-Fidelity Models*. Comment: 33 pages, 13 figures. The paper is under review. Apr. 2023. DOI: 10.48550/arXiv.1609.07196 (cit. on p. 10).

[136] K. Cheng et al. "Surrogate-Assisted Global Sensitivity Analysis: An Overview." In: *Structural and Multidisciplinary Optimization* 61.3 (Mar. 2020), pp. 1187–1213. DOI: 10.1007/s00158-019-02413-5 (cit. on p. 10).

[137] D. G. Krige. "A statistical approach to some basic mine valuation problems on the Witwatersrand." In: *Journal of the Southern African Institute of Mining and Metallurgy* 52.6 (Dec. 1951), pp. 119–139. DOI: 10520/AJA0038223X_4792 (cit. on p. 10).

[138] G. Matheron. "Principles of geostatistics." In: *Economic Geology* 58.8 (Dec. 1963), pp. 1246–1266. DOI: 10.2113/gsecongeo.58.8.1246 (cit. on p. 10).

[139] P. D. Thompson. "Optimum Smoothing of Two-Dimensional Fields." In: *Tellus* 8.3 (Jan. 1956), pp. 384–393. DOI: 10.3402/tellusa.v8i3.9008 (cit. on p. 10).

[140] J. Sacks et al. "Design and Analysis of Computer Experiments." In: *Statistical Science* 4.4 (1989), pp. 409–423 (cit. on p. 10).

[141] M. D. McKay, R. J. Beckman, and W. J. Conover. "Comparison of Three Methods for Selecting Values of Input Variables in the Analysis of Output from a Computer Code." In: *Technometrics* 21.2 (May 1979), pp. 239–245. DOI: 10.1080/00401706.1979.10489755 (cit. on p. 10).

[142] D. P. Kingma and J. Ba. *Adam: A Method for Stochastic Optimization*. Jan. 2017. DOI: 10.48550/arXiv.1412.6980 (cit. on p. 10).

[143] J. N. Fuhg, A. Fau, and U. Nackenhorst. "State-of-the-Art and Comparative Review of Adaptive Sampling Methods for Kriging." In: *Archives of Computational Methods in Engineering* 28.4 (June 2021), pp. 2689–2747. DOI: 10.1007/s11831-020-09474-6 (cit. on p. 12).

[144] M. Schonlau. "Computer Experiments and Global Optimization." PhD Thesis. Canada: University of Waterloo, 1997 (cit. on p. 12).

[145] M. Schonlau, W. J. Welch, and D. R. Jones. "Global versus Local Search in Constrained Optimization of Computer Models." In: *Lecture Notes-Monograph Series* 34 (1998), pp. 11–25 (cit. on p. 12).

[146] J. Gardner et al. "Bayesian Optimization with Inequality Constraints." In: *Proceedings of the 31st International Conference on Machine Learning*. Ed. by E. P. Xing and T. Jebara. Vol. 32. Proceedings of Machine Learning Research 2. Bejing, China: PMLR, June 2014, pp. 937–945 (cit. on pp. 12, 15).

[147] L. Laurent. "Stratégie multiparamétrique et métamodèles pour l'optimisation multiniveaux de structures." PhD Thesis. Cachan, Ecole normale supérieure, Dec. 2013 (cit. on p. 13).

[148] C. Sabater, P. Bekemeyer, and S. Görtz. "Efficient Bilevel Surrogate Approach for Optimization Under Uncertainty of Shock Control Bumps." In: *AIAA Journal* 58.12 (Dec. 2020), pp. 5228–5242. DOI: 10.2514/1.J059480 (cit. on p. 13).

[149] S. Bagheri et al. "Constraint handling in efficient global optimization." In: *Proceedings of the Genetic and Evolutionary Computation Conference*. GECCO '17. New York, NY, USA: Association for Computing Machinery, July 2017, pp. 673–680. DOI: 10.1145/3071178.3071278 (cit. on p. 15).

[150] J. Ungredda and J. Branke. *Bayesian Optimisation for Constrained Problems*. May 2021. DOI: 10.48550/arXiv.2105.13245 (cit. on p. 15).

[151] B. Balaram, M. D. Narayanan, and P. K. Rajendrakumar. "Optimal design of multi-parametric nonlinear systems using a parametric continuation based Genetic Algorithm approach." In: *Nonlinear Dynamics* 67.4 (Mar. 2012), pp. 2759–2777. DOI: 10.1007/s11071-011-0187-z (cit. on p. 15).

[152] G. Duffing. "Erzwungene Schwingungen bei veränderlicher Eigenfrequenz und ihre technische Bedeutung." In: *Sammlung Vieweg*. Vol. 41–42. Braunschweig: F. Vieweg & Sohn, 1918 (cit. on p. 15).

[153] I. Kovacic and M. J. Brennan. *The Duffing Equation: Nonlinear Oscillators and their Behaviour*. Chichester: John Wiley & Sons, Feb. 2011. DOI: 10.1002/9780470977859 (cit. on p. 15).

[154] D. Williams and D. A. Lang. "Analysis of a Gantry Crane for Severe Seismic Criteria." In: *Proceedings of the Seventh World Conference on Earthquake Engineering*. Vol. 8. Istanbul, Turkey, 1980, p. 459 (cit. on p. 22).

[155] Association Française de Normalisation (AFNOR). *NF EN 1998-1: Eurocode 8: Design of structures for earthquake resistance - Part 1 : general rules, seismic actions and rules for buildings*. Paris, Jan. 2010 (cit. on p. 24).

[156] Hilti. *PROFIS Engineering Suite*. Hilti. 2022 (cit. on p. 25).

[157] Association Française de Normalisation (AFNOR). *NF EN 1992-4: Eurocode 2: Design of concrete structures - Part 4 : design of fastenings for use in concrete*. Paris, Feb. 2019 (cit. on p. 25).

[158] L. Xie et al. "Bifurcation tracking by Harmonic Balance Method for performance tuning of nonlinear dynamical systems." In: *Mechanical Systems and Signal Processing* 88 (May 2017), pp. 445–461. DOI: 10.1016/j.ymssp.2016.09.037 (cit. on p. 32).

[159] L. Xie et al. "Numerical Tracking of Limit Points for Direct Parametric Analysis in Nonlinear Rotordynamics." In: *Journal of Vibration and Acoustics* 138.2 (Jan. 2016), p. 021007. DOI: 10.1115/1.4032182 (cit. on p. 32).

[160] Q. Ragueneau, L. Laurent, and A. Legay. *BO-HBM-ex*. Version v1.0.4. Dec. 2023. DOI: 10.5281/zenodo.10259290 (cit. on p. 33).